Astroglia-derived TIMP-1 alleviates cognitive deficits by restoring synaptic plasticity in Alzheimer's disease

Sukanya Sarkar[1], Kusumika Gharami[1], Ramesh Kumar Paidi[1,2], B.N. Srikumar[3], Subhas C. Biswas[1,4,*]

[1]Cell Biology and Physiology Division, CSIR-Indian Institute of Chemical Biology, 4 Raja S. C. Mullick Road, Kolkata 700 032, India; [2]Current address: Department of Neurological Sciences, RUMC, 1735 West Harrison St, Suite Cohn 336, Chicago, IL 60612, USA; [3]Department of Neurophysiology, National Institute of Mental Health and Neuro Sciences (NIMHANS) Hosur Road, Bengaluru – 560029, India; [4]Lead contact.

[*] To whom correspondence should be addressed: Subhas C Biswas, Cell biology and Physiology Division, CSIR-Indian Institute of Chemical Biology, 4 Raja S. C. Mullick Road, Kolkata 700 032, India. Phone: 91-33-24995941. FAX: 91-33-24735197. E-mail: biswassc@gmail.com; subhasbiswas@iicb.res.in

Abstract

Astrocytes respond to any pathological insult to brain including Alzheimer's disease (AD) through 'reactive astrogliosis'. Recently, we demonstrated that tissue inhibitor of matrix metalloproteinase-1 (TIMP-1), a neuroprotective cytokine, is released through reactive astrogliosis early in response to amyloid-β (Aβ). Here, we show that TIMP-1 has superior mechanism-of-actions on neurons in models of AD. It not only confers neuroprotection against Aβ-induced apoptosis and autophagy via CD63 receptor but also displays synapse–specific effects that underlie cognitive recovery in AD. We detect diminished levels of TIMP-1 in the hippocampi of 5xFAD mice versus wild-type counterparts. Interestingly, exogenous TIMP-1 injection in this transgenic model ameliorates its cognitive functions, likely by restoring long-term potentiation at hippocampal synapses. We observe BDNF induction and GSK3β inhibition, which may be the key TIMP-1-driven underlying mechanisms at synapses. Thus, we show an astrocyte-origin cytokine-driven mechanism for synaptic and cognitive salvation promising an exciting avenue in AD therapeutic research.

Key words: Reactive astrocytes, astrogliosis, Alzheimer's disease, Aβ, synaptic plasticity, apoptosis, autophagy, cytokine, neuroprotection

Competing Interest Statement

The authors have declared no competing interest.

INTRODUCTION

Alzheimer's disease (AD) is the most dreaded multi-factorial neurodegenerative disorder with no effective cure to date. This calls for integrated studies of neurons with glia in AD research. Astrocytes, the most abundant of the glial cells, are now considered critical in the progress of neurodegenerative diseases including AD besides their indispensable homeostatic functions in the CNS[1,2]. Astrocyte reactivity[3] gives rise to a heterogeneous population of reactive astrocyte subtypes. Initially, classified into detrimental – A1 (LPS treatment) and beneficial – A2 (ischemic stress) subtypes[4]; recent reports unveiled a plethora of reactive astrocytes existing across diseases and disease-stages. While a disease-associated astrocyte (DAA) subtype was detected in AD[5], more recent delineation of astrocyte subtypes in a lipopolysaccharide-injected inflammatory mouse model provides critical insights into location-specific reactive astrocyte populations in brain[6]. The kinetics of astrocyte reactivity *in vitro* in response to Aβ treatment was reported by us and analysis of the astrocyte-conditioned media revealed time dependent differential enrichment of pro- and anti-inflammatory cytokines among which tissue inhibitor of matrix metalloproteinase 1 (TIMP-1) emerged as one of the major neuroprotective cytokines[7].

TIMP-1, extensively studied in cancer, has gained some limelight in neurodegenerative diseases[8-10]. TIMP-1 is almost exclusively expressed by astrocytes in white matter lesion and plays a neuroprotective role by inhibiting matrix metalloproteinase (MMP) activities[11]. Indeed, a TIMP-1-expressing reactive astrocyte subtype was detected in white matter tracts of a lipopolysaccharide-induced mouse model with suggested participation in extracellular matrix remodelling, neuroprotection and remyleination[6]. TIMP-1 and MMP levels greatly vary in the plasma between neurodegenerative disorder patients and healthy controls signifying the importance to study TIMP-1 in neurodegenerative disorders[12]. However, several reports suggest an MMP-independent role of TIMP-1[13]. The versatility of TIMP-1 is due to its two-domain structure – N-terminal domain responsible for MMP inhibition and C-terminal domain (CTD) for cytokine-like cellular signaling. The multi-functionality of TIMP-1 arises from the competition among its different binding partners for their corresponding attachment domain which is influenced by context, TIMP-1:MMP ratio, and binding affinities of the partners. When TIMP-1 level is higher than MMPs, free uncomplexed TIMP-1 molecules are available to bind to cognate cell-surface receptors such as CD63[14], CD82[15] and LRP-1[16], through its CTD, inducing

downstream signaling pathways. Furthermore, during pathological insult, when the levels of MMPs are higher than TIMP-1, MMP-9 activity increases[17]; more pro-MMP9s, initially occupying TIMP-1's CTD, are cleaved into MMP-9 and therefore the CTD becomes free for binding and signaling through CD63 via integrinβ1, MAPK[14], FAK[18] and PI3K/Akt[19,20] pathways. Thus, TIMP-1 under both these situations induces intracellular signaling. Therefore, TIMP-1 emerges as an astroglia-derived neuroprotective molecule but its main mechanism-of-action on neurons from an intracellular signaling perspective remains incompletely understood.

In this study, we observed salvation of cognitive deficits in 5xFAD mouse model of AD with TIMP-1. We detected the underpinning intracellular mechanisms especially the synaptic changes driven by TIMP-1 in rescuing cognitive malfunctions in 5xFAD mouse; identifying the major cellular mediators of its modus operandi.

RESULTS

TIMP-1 injection rescues cognitive deficits in 5xFAD mice

5xFAD mouse starts developing Aβ plaques at 2 months, inducing extensive reactive astrogliosis, microgliosis, and eventually synaptic and neuronal loss[21]. We first checked the levels of TIMP-1 (secreted form, 25 kDa) in the 5xFAD mice versus wild type C57/BL6 mice (WT) across different age groups. TIMP-1 was markedly reduced in the hippocampal (Figures 1A and 1B, Figures S1A and 1B) and cortical tissues (Figures S1C and S1D) of 2-month (M), 4M, 6M, 8M and 10M-old 5xFAD mice in western blot (WB) analyses compared to age-matched WT groups. There was four-fold reduction in TIMP-1 expression compared to WT from 6M onwards in the hippocampus. Hence, TIMP-1 injection and all subsequent experiments were performed in 6M-old 5xFAD mice. This suggests that intracerebroventricularly (i.c.v.) injected TIMP-1 (Figure 1C) directly and majorly contributes to the changes subsequently observed in the 5xFAD mice, without significant contribution from endogenous TIMP-1. Diffusion of TIMP-1 by 8 days following i.c.v. injection, in the hippocampal and cortical regions of 5xFAD mouse, was confirmed by immunofluorescence studies (Figures 1D and 1E).

Following TIMP-1 injection, a battery of behavioral tests was performed to check the effect of TIMP-1 on cognitive behaviors of 5xFAD mice. In open-field test (OFT), both 5xFAD and artificial cerebro-spinal fluid (aCSF)-injected 5xFAD mice displayed hyper-locomotion (Figures

1F and 1G; Figure S2A) and decreased thigmotactic behavior (Figures 1F and 1H and Figure S2B) suggesting increased anxiety that were significantly attenuated by TIMP-1 (5 ng) as represented by the average distance travelled (in cm) and the time spent in the outer zone (sec) by mice in each group in the 10 min period. In elevated-plus maze (EPM) test (schema in Figure 1I), there was no significant difference between the initial transfer latency (ITL) on Day-1 and retention transfer latency (RTL) on Day-2 in the 5xFAD and 5xFAD+aCSF groups while in both WT and TIMP-1-treated 5xFAD groups RTLs were reduced significantly compared to ITLs (Figure 1J, Figure S2C). Mean ITL-RTL values are additionally represented for each group (Figure 1J; Figure S2D), showing that TIMP-1 treatment significantly improved ITL-RTL score in 5xFAD mice (positive value) compared to the untreated 5xFAD group (negative value) indicating that 5xFAD mice display a better memory retention following TIMP-1 treatment. In novel object recognition (NOR) test (schema for Day-2 with novel (N) and familiar (F) objects in Figure 1K), both 5xFAD and 5xFAD+aCSF mice spent significantly shorter time with novel object than that with familiar object on Day-2 (Figure 1L; Figure S2E), further evidenced by negative values for Discrimination index (DI; Figure 1M) and <50% score in Preference index (PI; Figure 1N). TIMP-1 treatment significantly improved the novel object exploration time of 5xFAD mice on Day-2 (Figure 1L; Figure S2E), depicted further with positive DI value (Figure 1M) and >50% PI score (Figure 1N). TIMP-1 therefore ameliorated long-term recognition memory in 5xFAD mice. Figures 1O and 1Q show schemas for contextual fear conditioning (CFC) and cue-dependent fear conditioning (CDFC) (Day-1 acquisition) tests respectively. In both the tests, average % freezing of a mouse in 8 min encompassing the four test sessions on Day-2 (see materials and methods) was calculated. On Day-2 of CFC, the 5xFAD and 5xFAD+aCSF mice displayed a diminished retention of context-dependent fear memory, that is, reduced % freezing value versus WT mice that was significantly improved in the TIMP-1-treated 5xFAD group (Figure 1P). Coherently, cue-dependent fear memory was significantly disrupted in the 5xFAD and 5xFAD+aCSF mice on Day-2 of CDFC and corrected by TIMP-1 injection (Figure 1Q). The results indicate a role of TIMP-1 in better retention of fear memory that involves astute coordination between hippocampus and amygdala. Additionally, we checked the changes in Aβ plaque deposition 14 days post TIMP-1 treatment. Both Aβ plaque burden and plaque number were significantly reduced by TIMP-1 injection in 5xFAD mice (Figures S3A-S3C). Altogether, these data suggest that TIMP-1 detected at drastically reduced levels in 6M-

old 5xFAD mice coincide with enhanced Aβ plaque deposition and cognitive deficits, both of which are reversed by recombinant TIMP-1 injection in the mice.

TIMP-1 binds to CD63 on neurons mediating Akt phosphorylation

CD63 is responsible for TIMP-1-mediated Akt signaling[22] (Schema in Figure 2A). We have shown that Akt is involved in TIMP-1-induced neuroprotection against Aβ toxicity[7]. Immunofluorescence staining for TIMP-1 (red) and CD63 (green) 16 h following TIMP-1 (100 ng/ml) addition to primary cortical neurons showed significantly enhanced co-localization between the two proteins (Figure 2B) on the neuronal surface quantified by Pearson correlation coefficient (Figure 2C).

To investigate the role of CD63 in TIMP-1-mediated Akt phosphorylation in primary neurons (schema in Figure 2D), we acquired CD63 siRNA (siCD63) and validated its efficacy (Figures 2E and 2F) 72 h following treatment. Expectedly, Akt phosphorylation was attenuated at 16 h post Aβ treatment compared to control cells and reversed significantly by TIMP-1 addition to Aβ-treated neurons (Figures 2G and 2H). Interestingly, upon CD63 downregulation, the improvement in Akt phosphorylation induced by TIMP-1 against Aβ was lost. Hence, we interpret that CD63 receptor is not only responsible for the binding of TIMP-1 on neuronal surface but is additionally required for mediating TIMP-1-directed Akt phosphorylation at Ser473.

TIMP-1 restricts nuclear translocation of FOXO3a and related apoptotic signaling induced by Aβ

Aβ treatment to cortical neurons causes dephosphorylation of Akt and its downstream target FOXO3a. Dephosphorylated FOXO3a(S253) translocates to the nucleus increasing transcription of pro-apoptotic genes *Bim*[23] and *Puma*[24] (Schema in Figure 3A). We found that TIMP-1 restored the phosphorylation of FOXO3a(S253) in Aβ-treated primary neurons at 16 h following treatment (Figures 3B and 3C) while the total FOXO3a and actin levels remained unaltered across the treatment conditions. Consistently, FOXO3a puncta (green) that were increased in the nuclei (blue) of Aβ-treated neurons, 16 h post treatment, indicating FOXO3a's nuclear localization were attenuated by TIMP-1 treatment (Figures 3D and 3E). FOXO3a-induced pro-apoptotic proteins BIM (Figures 3F and 3G) and PUMA (Figures 3F and 3H) were significantly

upregulated in Aβ-treated neurons but markedly reduced under Aβ+TIMP-1 co-treatment (Figures 3F-H). Interestingly, anti-apoptotic protein Bcl-2 level, decreased in Aβ-treated neurons, was elevated upon TIMP-1 treatment (Figures 3F and 3I) while another anti-apoptotic protein Bcl-xL, remained unchanged across the treatment conditions (Figures 3F and 3J). Notably, Bcl-2 and Bcl-xL levels are differentially regulated in response to TIMP-1 in different disease models and stages[8,25,26]. Coherently, pro-apoptotic BAX (Figures 3F and 3K), DNA damage marker pH2Ax (Figures 3F and 3L) and apoptotic effector - cleaved Caspase3 (Figures 3F and 3M) levels were down-regulated in Aβ+TIMP-1-treated cells contrary to Aβ-treated neurons. Expectedly, TUNEL assay in coronal brain sections revealed a significant increment in the number of TUNEL positive (apoptotic) cells in the hippocampal regions of 5xFAD mice compared to WT in immunofluorescence studies, which were significantly reduced 14 days post TIMP-1 treatment (Figures S4A and S4B). Furthermore, TIMP-1 abrogated the high levels of pH2Ax in 5xFAD mice determined by WB analyses of whole hippocampal tissue (Figures S4C and S4D) and immunofluorescence studies of hippocampal (Figures S4E and S4F) and cortical sections (Figures S4G and S4H). Thus, TIMP-1 protects neurons against Aβ toxicity by inhibiting apoptosis along Akt/FOXO3a/BIM/PUMA axis.

TIMP-1 corrects impaired autophagy flux in Aβ-treated primary neurons and in 5xFAD mice

Our lab has shown earlier that Aβ treatment to primary cortical neurons simultaneously induces both apoptosis and aberrant autophagy showing accumulation of autophagic proteins in neurons, preventing their clearance and leading to impaired autophagy flux[27,28](schema in Figure 4A). Therefore, here we investigated the effect of TIMP-1 on impaired autophagy flux, induced by Aβ, in neurons. We found increased levels of ATG5 (an upstream marker for elongation of autophagosome, Figures 4B and 4C), p62 (cargo adaptor and the most crucial determinant of autophagy flux, Figures 4D and 4E) and LC3B-II (Figures 4F and 4G) following Aβ treatment through WB analyses of primary neuron lysates. Lysosome numbers were up-regulated, identified by lysosome-marker LAMP1 level in Aβ-treated neurons indicating that although autophagy was induced by Aβ, the flux was eventually impaired (Figures 4H and 4I). TIMP-1 addition to Aβ-treated neurons improved autophagy flux by reversing the levels of ATG5, p62, LC3BII and LAMP1 to the control levels (Figures 4B-4I). Immunofluorescence analyses of p62

(Figures 4J and 4K), LC3B (Figures 4L and 4M) and LAMP1 (Figures 4N and 4O) levels under same conditions 16 h post-treatment corroborated the WB results. Hence, both apoptosis and autophagy are regulated by TIMP-1 through phosphorylation of a common upstream kinase, Akt, protecting cells against Aβ toxicity.

In vivo, TIMP-1 upregulated inhibitory phosphorylation of ULK-1 at S757 that likely prevented autophagy induction in 5xFAD mouse hippocampus (Figures S5A and S5C) and cortex 14 days post treatment (Figures S5B and S5D). Enhanced levels of p62 (Figures S5E-S5H), LC3B (Figures S5I-S5L) and LAMP1 (Figures S5M-S5P) in 5xFAD mice in immunofluorescence studies indicated that although autophagy was induced in 5xFAD mice, the pathway was eventually impaired leading to increased accumulation of autophagosomes and lysosomes in the transgenic mouse brain that were ameliorated by TIMP-1 treatment, corroborating the *in vitro* results.

TIMP-1 improves pre- and post-synaptic protein expressions in 5xFAD mice

Next, we investigated the underlying direct mechanisms, that is, the synaptic underpinnings of the cognitive improvement observed in TIMP-1-treated 5xFAD mice. Pre- and post-synaptic protein levels, common determinants of synaptic health, were checked in whole tissue and in synaptosomes (Figure 5A). TIMP-1 injection in 5xFAD mouse induced two-fold increase in pre-synaptic SNAP25 fluorescence intensities in the CA1 hippocampi (Figures 5B and 5C) and cortices (Figures S6A and S6B) compared to untreated 5xFAD mice. Coherently, post-synaptic marker PSD95 intensities were also enhanced in the CA1 hippocampi (Figures 5D and 5E) and cortices (Figures S6C and S6D) of 5xFAD+TIMP-1 mice. WB analyses of whole hippocampal tissue from TIMP-1-treated 5xFAD mice further corroborated the improvement in SNAP25 (Figures 5F and 5G) and PSD95 (Figures 5H and 5I) levels compared to 5xFAD group. However, no significant changes were observed in these synaptic protein levels in whole cortex from 5xFAD+TIMP-1 group (data not shown). No significant change was observed across groups in hippocampus for additional synaptic markers - Synaptophysin-1(pre-synaptic) and Homer-I(post-synaptic) (Figures S6E and S6F).

In order to delineate the changes mediated by TIMP-1 specifically at the synapse, we utilized synaptosome preparations. Pre-synaptic nerve terminals in synaptosomes often remain attached

with the post-synaptic membrane and the post-synaptic density proteins[29]. WB analyses with viable synaptosomes from the four treatment groups of mice – WT, 5xFAD, WT+TIMP-1 and 5xFAD+TIMP-1 revealed that the expressions of pre-synaptic (Figures 5J-5L) and post-synaptic (Figures 5J, 5M and 5N) markers were significantly lower in 5xFAD mice compared to WT mice both in the cortical and hippocampal regions. Fourteen days post TIMP-1 treatment the level of SNAP25 (Figures 5J and 5K) and PSD95 (Figures 5J and 5M) were significantly improved in cortices and hippocampi of 5xFAD mice. TIMP-1 did not significantly improve the synaptophysin-1 level in cortical nor in hippocampal 5xFAD synapses (Figures 5J and 5L). Unlike whole tissue results, HOMER-1 level was significantly improved in the 5xFAD+TIMP-1 mouse cortex but not in hippocampus (Figures 5J and 5N). No significant change was observed in synaptic protein expressions with TIMP-1 treatment to WT mice. Altogether, these results suggest that TIMP-1 was able to improve specific synaptic protein levels in 5xFAD mice.

TIMP-1 ameliorates deficits in synaptic spine density and spine size in 5xFAD mice

Dendritic spines, constituting the majority of excitatory synapses, are highly dynamic in their size, shape and density, and their changes are strongly correlated with learning and memory functions[30]. Golgi-cox staining and imaging of brain slices (Figure 6A) 14 days post TIMP-1 injection in 5xFAD mice revealed significant increase in spine density (number of spines/10 µm) in hippocampal (CA1) (Figures 6B and 6C) and cortical regions (Fig 6B and 6D) compared to untreated 5xFAD mice. The spine density remained unaltered between the WT and WT+TIMP-1 groups.

Besides synaptic spine density, spine size is another morphological aspect of synapses that is altered in an activity-dependent form of plasticity. Spine shrinkage is a well-studied abnormality in AD[31]. Changes in spine size are regulated by dynamic alterations in the cytoskeletal actin content[32] quantifiable by the ratio of filamentous (F) versus globular (G) forms of actin in synaptosome. We fractionated viable synaptosomes into the cytoskeletal fraction constituting F actin and the supernatant fraction constituting G actin (Figure 6E). F/G actin ratio was significantly reduced in the hippocampal synaptosome sub-fractions from 5xFAD mice compared to WT group. TIMP-1 improved the spine cytoskeletal actin content in 5xFAD mice, indicated by an increased F/G actin ratio (Figures 6F and 6G). Furthermore, no significant

alteration was observed in the cortical synaptosomal actin contents among the treatment groups (Figures 6F and 6H). Spine shape and maturation are correlated to the stabilization of actin cytoskeleton. Phosphorylation of Cofilin (actin-binding protein) is a major regulator for the stabilization of actin cytoskeleton and thereby helps spines to attain maturation followed by spine enlargement[33]. Phosphorylated Cofilin(S3) levels were approximately 50% lower in 5xFAD mice compared to WT mice, both in the hippocampus (Figures 6I and 6J) and cortex (Figures 6I and 6K), that were significantly improved by TIMP-1, indicating that TIMP-1 helps in inducing spine maturation and consequent improvement in spine shape, more specifically at hippocampus.

TIMP-1 induces BDNF and related signaling in 5xFAD mice

TIMP-1 improved synaptic health. Hence, we questioned whether this effect was direct or indirect by induction of any neurotrophin namely brain-derived neurotrophic factor (BDNF), the most important determinant neurotrophin in spine health[34] and synaptic plasticity[35]. We found four-fold reduction in Pro-BDNF level, precursor of BDNF, in the whole hippocampal lysates of 5xFAD mouse compared to WT animal. Fourteen days post TIMP-1 treatment, Pro-BDNF level improved in 5xFAD mouse up to the WT level (Figures 7A and 7B). CREB is the specific transcription factor that promotes *Bdnf* gene expression and pCREB(S133)/CREB/BDNF axis is known to be deregulated in AD[36]. In coherence to BDNF results, we observed a similar increase in pCREB(S133)/CREB expressions in 5xFAD+TIMP-1 mice versus 5xFAD mice (Figures S7A and S7B). This excited us to investigate the effect of TIMP-1 on BDNF-TrkB signaling pathways implicated in synaptic plasticity, namely, PI3K/Akt and ERK/MAPK pathways[37]. However, TrkB, cognate receptor of BDNF, both in its full length (fl-TrkB) (Figures 7C and 7D) and truncated (t-TrkB) (Figures 7C and 7E) isoforms were not significantly altered in the hippocampus. Expectedly, Akt phosphorylation was improved at Ser473 in TIMP-1-injected 5xFAD mouse (Figures 7F and 7G) compared to untreated 5xFAD mouse in consistence with our *in vitro* results but additionally at Thr308 (Figures 7H and 7I), whereas, phosphorylation levels of ERK1 (Figures 7J and 7K) and ERK2 (Figures 7J and 7L), were unchanged indicating that the ERK pathway remained unaltered.

Pro-BDNF level in isolated synaptosomes from adult mouse is a measure of the release-ready intra-synaptic secretory (vesicular) pool of BDNF's precursor form. We detected almost 50% reduction in pro-BDNF level at hippocampal (Figures 7M and 7N) and 20% at cortical (Figures S8A and S8B) synapses in 5xFAD mouse. TIMP-1 improved the levels significantly in both regions. However, TrkB (fl-TrkB and t-TrkB) remained unaltered across treatment groups in hippocampal (Figures 7O-7Q) and cortical (Figures S8C-S8E) synaptosomes like in total tissues. Further, we found improved phosphorylation of Akt at Ser473 (Figures 7R and 7S) but not at Thr308 (Figures 7T and 7U) in the hippocampal synaptosomes from TIMP-1-treated 5xFAD mice compared to untreated 5xFAD animals, indicating that although Akt signaling is induced at synapses by TIMP-1 treatment, not all its active sites are equally phosphorylated. In cortical synapses, we detected similar level of improvement in pAkt(S473) expression in 5xFAD+TIMP-1 group compared to 5xFAD group (Figures S8F and S8G) but there was no change in the pAKT(T308) level among groups (Figures S8H and S8I). Conversely, unlike total hippocampal level, we observed significant reductions in pERK1/ERK2 (Figures 7V and 7W) and pERK2/ERK2 (Figures 7V and 7X) levels in the hippocampal synapses from 5xFAD mice, that were improved upon TIMP-1 treatment indicating that alterations in ERK activation could be detected at the synaptic level and not in the whole tissue level. A similar recovery in both pERK1/ERK2 (Figures S8J and S8K) and pERK2/ERK2 (Figures S8J and S8L) levels was observed at cortical synapses.

TIMP-1 improves basal synaptic transmission and long-term potentiation in the hippocampal schaffer collateral-CA1 synapses in 5xFAD mice

BDNF induces long-term potentiation (LTP) in hippocampus[38]. LTP/LTD regulation forms the basis of synaptic plasticity that underlies learning and memory[39]. Hence, we investigated whether TIMP-1 treatment evoked LTP induction in 5xFAD model. A schema of the *ex vivo* electrophysiology at Schaffer collateral-CA1 synapses in mouse hippocampus is shown in Figure 8A. First, we checked whether basal synaptic transmission was affected at Schaffer collateral-CA1 synapses in 5xFAD mice compared to WT mice using input-output (I-O) relationship. Figure 8B shows representative fEPSP traces along increasing current stimulus intensities (20 – 300 µA with 20 µA increments), from each experimental group. In 5xFAD slices, the fEPSP response at all current intensities was lower than that in WT slices. TIMP-1 improved the fEPSP

slope values in 5xFAD mouse significantly at several current intensities, the highest being at 260 µA (Figure 8C). Area under curve (AUC) analysis for Figure 8C corroborated the reduced basal transmission observed in 5xFAD mice and its significant improvement upon TIMP-1 treatment (Figure 8D).

Next, we studied the effect of TIMP-1 treatment to 5xFAD mice on short-term plasticity by determining the paired-pulse facilitation (PPF) ratio at the Schaffer collateral-CA1 synapses. PPF helps in evaluating the alterations in pre-synaptic activity and neurotransmitter release probability by delivering two consecutive stimulating pulses with a short inter-stimulus interval (ISI). PPF ratio remained unaltered among the experimental groups (Figure 8E), further corroborated by AUC calculation (Figure 8F). Thus, the probability of pre-synaptic neurotransmitter release did not differ between WT and 5xFAD mice in the hippocampal SC-CA1 synapses, with no further change upon TIMP-1 treatment.

We evaluated synaptic potentiation at three different plasticity time points – Post-tetanic potentiation (PTP, 3min post theta burst stimulation (TBS)), short-term potentiation (STP, 21st-30th min post TBS) and LTP (41st-60th min post TBS i.e. early-phase LTP). Figures 8G shows the time course of normalized fEPSP response of the treatment groups, 20 min before and 60 min after TBS. Figures 8H shows the representative tracings of pre- and post-TBS fEPSPs in each group. AUC of the total time course of fEPSP responses in 5xFAD slices was significantly decreased compared to WT slices while AUC in 5xFAD+TIMP-1 group was comparable to WT and WT+TIMP-1 groups (Figure 8I). No significant change was detected in PTP (Figure 8J) and STP (Figure 8K) responses among the treatment groups. Conversely, LTP induction was found to be significantly lower in the 5xFAD hippocampal slices compared to WT mice. TIMP-1 injection in 5xFAD mice significantly improved the level of LTP induction while LTP induction remained similar between WT and WT+TIMP-1 slices (Figure 8L).

GSK3β is an important regulator of LTP/LTD signaling implicated in synaptic changes in the brain[40] and plays a critical role in AD[41]. Since we found LTP induction with TIMP-1 treatment to 5xFAD mice, we hypothesized that TIMP-1 may have a role in GSK3β signaling. We found increased GSK3β phosphorylation at Ser9, indicating GSK3β inhibition, in whole tissue (Figures 8M and 8N) and synaptosomal lysates from hippocampi of TIMP-1-treated 5xFAD mice

compared to low inhibitory phosphorylation level in untreated 5xFAD mice indicating GSK3β activation (Figures 8M and 8O).

DISCUSSION

Our research[7] in consistence with several reports[42,43] indicates that reactive astrocytes in AD can be an excellent source of disease-modulating cytokines whose detailed mechanism-of-actions are incompletely understood. In this study, we revealed the underlying key molecular mechanisms of TIMP-1, an astroglia-derived Aβ-responsive anti-inflammatory cytokine, identified by us earlier[7], on neuroprotection, synaptic efficacy and cognitive salvation in AD. We found that endogenous TIMP-1 level is very low in the hippocampus of a transgenic model of AD, 5xFAD mouse, compared to WT mouse across age. Interestingly, intra-cerebroventricular injection of exogenous TIMP-1 in this mouse not only improved their long-term hippocampus-dependent contextual memory (explicit memory) but also rescued fear memories (implicit memory). While TIMP-1 ensured neuronal viability, by regulating two prominent yet intertwined cell-death pathways – apoptosis and autophagy by binding to its cognate receptor CD63, it also improved synaptic integrity and function – the direct cellular correlates of cognitive salvation. The latter effect may be attributed to an enhanced expression of BDNF and related signaling as well as GSK3β inhibition especially at synapses following TIMP-1 injection to 5xFAD mouse.

In 5xFAD mice, we detected lower endogenous TIMP-1 level than WT mice across age, earliest at 2 months, coinciding with an inherent early Aβ accumulation in this model. A study controversially showed that TIMP-1 increases significantly at 4 months in 5xFAD mice but fall to the WT level at 6 month of age[44]. Our results are however consistent with a strong body of evidence suggesting a biphasic regulation of TIMP-1 in response to acute versus chronic inflammatory insults associated with HIV-associated neurocognitive disorders (HAND)[9]. TIMP-1 was regarded as a neuroprotective molecule that decreases in CSF and tissue samples of HAND patients compared to healthy individuals but increases when acute inflammatory insult is given to primary astrocytes in culture[8,10], the latter consistent with our report[7]. Possibly, the early secretion of TIMP-1 in response to Aβ is an attempt by the astrocytes to protect and repair neuronal damage due to the insult but in case of prolonged presence of Aβ, as in aging 5xFAD mice, TIMP-1-mediated neuroprotection is lost due to the downregulation of TIMP-1 by an

unknown mechanism. Interestingly, transcriptomes of neurons derived from human induced pluripotent stem cells generated from skin fibroblasts of AD patients carrying mutation in *PSEN1* gene show downregulation of *Timp-1* gene[45], emphasizing TIMP-1's neuroprotective significance and alluding to a possible connection with AD-associated genes.

Our previous work shows that TIMP-1 can activate Akt[7] but the downstream cellular pathway/s effective against AD remained unexplored. Here, we demonstrate that CD63 is the specific receptor responsible for TIMP-1-driven Akt activation in Aβ-treated primary neurons utilizing co-localization and RNAi techniques. TIMP-1 via CD63 induces Akt signaling in many different cell types[19,20,22]. It is probably the most important binding partner for intracellular signaling as opposed to other competitive interactors of TIMP-1, especially when TIMP-1 is in excess and unbound[17] like the exogenous addition in our study. Since AD is a proteopathic disease where autophagy and apoptosis cooperate in mediating neurotoxicity[27,28] and Akt is a common upstream regulatory kinase[46], TIMP-1 likely mediates neuroprotection by manipulating this common regulatory point (phosphorylating Akt) for these interconnected cell death pathways in our AD models. Nevertheless, both apoptosis and autophagy regulations have direct implications in cognitive functioning which has not been explored here.

Progressive changes in synaptic structure and functions often precede the actual neuronal loss and memory deficits in AD[47,48]. We find that TIMP-1 not only ensures overall neuronal viability but also protects synaptic structures. It improves pre- and post-synaptic protein levels, spine density and size of synapses in 5xFAD mouse, compared to untreated one. Actin cytoskeleton plays a pivotal role in spine dynamics both from structural and functional perspectives. Notably, loss of F-actin occurs selectively at synapses at very early ages in a mouse model of AD (APPswe/PS1ΔE9), well ahead of the onset of pathological hallmarks and memory deficits in this model[49]. We show that F/G actin ratio was significantly improved in hippocampal synapses with TIMP-1 treatment in 5xFAD mice as opposed to untreated 5xFAD animals. We further provide evidence that TIMP-1 reduces the hyperactivated levels of cofilin (dephosphorylated Cofilin) in isolated synaptosomes from 5xFAD mice. Hyperactive cofilin in 5xFAD mouse is capable of forming rod-shaped actin/cofilin bundles in the cytoplasm of dendritic spine, blocking axonal trafficking and is responsible for synaptic dysfunctions leading towards synaptic loss in AD[50-53], which are likely prevented by TIMP-1. Our observations suggest that TIMP-1 has an

important role in regulating synaptic dynamics. However, not all the synaptic markers are sensitive to TIMP-1 treatment in 5xFAD mice which is consistent with previous reports on differential responses of synaptic proteins in AD brain[54-56].

Reduced release of BDNF in brain and blood are key determinants of pathological conditions in brain including AD[57,58]. In consistence with these reports, we detected significantly low levels of BDNF and BDNF-mediated signaling at hippocampal synapses in 5xFAD mice. TIMP-1 not only strongly improves BDNF level in 5xFAD mice but also enhances BDNF/TrkB-directed downstream Akt and ERK signaling pathways at these synapses. Our observations strengthen the ameliorative role of TIMP-1 specifically at synapses demonstrated by its ability to induce the expression of a well-recognized synaptically crucial neurotrophin.

A key finding of our study is the ability of TIMP-1 to improve LTP in 5xFAD mouse hippocampus. Previous studies have mostly shown cytokine-driven LTP suppression[59,60], constituting cytokine-driven neuroinflammation, as a contributing event in AD; here we demonstrate a cytokine-mediated beneficial upregulation of LTP in AD. Interestingly, TIMP-1 albeit via extracellular MMP-9 inhibition is required for both LTP maintenance[61] and late-phase LTP inhibition[62], the latter seen as a strategy to impede non-target late-phase LTP inductions and to ensure consolidation of the ongoing plasticity. We show that TIMP-1 contributes to early-phase LTP induction as a cell-signaling molecule triggering intracellular pathways. However, whether TIMP-1 has a local effect at synapses as a part of astrocyte-neuron communication is an open question. Interestingly, both PPR and PTP that measure changes in short-term plasticity and the probability of neurotransmitter release from the pre-synaptic terminals[63] remained unchanged across the treatment groups. Therefore, TIMP-1-driven improvement of LTP in hippocampus of 5xFAD mouse is probably independent of pre-synaptic activity. GSK3β is associated with PSD, regulates NMDAR-dependent synaptic plasticity[64] and NMDAR trafficking[65,66]. Increased GSK3β activity in AD[67] has the potential to negatively impact synaptic plasticity; in turn learning and memory[68]. GSK-3α and β are present within synapses[68]; more precisely, an electron microscopic study shows GSK-3β labeling of postsynaptic densities at dendritic spines[69]. Extrapolating from electrophysiological data, we predict that our observation of TIMP-1-mediated GSK3β inhibition in 5xFAD mice likely occurs at the post-synaptic compartment and not at the pre-synaptic terminal.

Our data demonstrate an ameliorative role of TIMP-1 at behavioral, viability and synaptic levels; however, the results collectively point to hippocampus as the main seat of action. Conversely, in some instances we did not find significant change in cortical whole tissues or synaptosomes. These results may be evidence of differential regulations at different brain regions or due to utilization of heterogeneous whole cortex tissues comprising affected and unaffected synaptic regions for WB analyses. Another interesting question would be to address the kinetics of Akt phosphorylation driven by TIMP-1 to divulge whether it is directly mediated by TIMP-1's signaling through CD63 or is it a downstream effect of TIMP-1-directed BDNF/TrkB signaling, or whether both occur simultaneously.

In conclusion, TIMP-1 emerges as a multi-functional cytokine released by reactive astrocytes at early stages in AD which not only protects neurons against apoptosis and autophagic deregulation but has a direct implication on several regulators of synaptic plasticity and this explains the mechanistic basis of TIMP-1-mediated cognitive recovery in 5xFAD mice. Two exciting revelations are (1) the notable extent of BDNF improvement observed upon exogenous TIMP-1 injection to 6-month-old 5xFAD mice that drastically lacks endogenous TIMP-1 and (2) TIMP-1-driven LTP induction. Broadly, our findings advance the role of TIMP-1 as a regulatory hub for several interconnected pathways[17] that impact cell functions at different levels which may be seen as a biological strategy[70] undertaken by astrocytes to ensure flexibility to adapt to changes in homeostasis as in AD. Altogether, our work promotes the efficacy of astroglia-derived TIMP-1 as an important candidate for potential therapeutic targeting for AD and possibly adds a step towards understanding cytokine-mediated astrocytic responses in neurodegenerative diseases.

METHODS

Experimental Design:

Multiple independent experiments were performed consisting of several biological replicates. Sample sizes and statistical analysis to calculate P values are given in detail in figure legends, in Supplementary Table 1 and in the 'Statistical analysis' section. No statistical method was followed to pre-determine the sample sizes but sample sizes were kept similar to that in relevant publications in literature. Data distribution was not formally tested for normality rather assumed

to be normal. Data were acquired and analyzed by multiple researchers, blind to the experimental conditions whenever experimentally feasible.

Materials:

Dulbecco's modified Eagle's medium (DMEM)-F12, Neurobasal medium, B27 supplement, Fetal Bovine Serum (FBS), goat serum, Penstrep antibiotic, Lipofectamine 2000, siCD63, scrambled siRNA (negative control), Sypro Ruby, Hoechst 33342, Prolong Gold Antifade with DAPI and Alexa Fluor were purchased from Thermo Fisher Scientific (MA, USA). Insulin, progesterone, putrescine, selenium, Apo-transferrin, poly-D-lysine (PDL), Di-methyl sulfoxide (DMSO), paraformaldehyde (PFA), bovine serum albumin (BSA), Triton-X 100, radioimmunoprecipitation assay (RIPA) buffer and 1,1,1,3,3,3 hexafluoro-2-propanol (HFIP) were purchased from Sigma-Aldrich (St. Louis, USA). Cell culture dishes, plates, filter units and flasks were purchased from BD Falcon (Schaffhausen, Switzerland) and Corning (NY, USA). Aβ (1–42) was purchased from Alexotech (Vasterbotten County, Sweden). PVDF membrane and Percoll were purchased from GE Healthcare (Buckinghamshire, UK). Enhanced chemiluminescence (ECL) substrate and stripping buffer were purchased from Takara Bio (Kusatsu, Japan). Sodium dodecyl sulphate (SDS) was purchased from Merck (Darmstadt, Germany). Trypsin and Bovine Serum Albumin (BSA) were purchased from Sisco Research Laboratories Pvt. Ltd (Mumbai, India). All other fine chemicals were procured from standard local suppliers unless stated otherwise. List of antibodies used for this work, their dilutions for each type of application and sources are given in the table below.

Antibody	Species raised	Application	Dilution	Source	Cat No.
phospho-Akt (S473)	rabbit	WB	1:500	CST	4058S
phospho-Akt (T308)	rabbit	WB	1:500	CST	4056S
Akt	rabbit	WB	1:1000	CST	9272S
phospho-FOXO3a (S253)	rabbit	WB	1:500	CST	9466S
FOXO3a	rabbit	ICC	1:100	CST	2497S
		WB	1:1000		
BIM	rabbit	WB	1:1000	Abcam	ab7888

PUMA	rabbit	WB	1:1000	Novus biologics	NBP1-76639
Bcl2	rabbit	WB	1:1000	CST	2870S
Bcl-xl	rabbit	WB	1:1000	CST	2762S
Bax	rabbit	WB	1:1000	CST	2772S
pH2Ax (S139)	rabbit	IHC	1:100	CST	9718S
		WB	1:1000		
Cleaved Caspase 3 (N175)	rabbit	WB	1:1000	CST	9661S
ATG5	rabbit	WB	1:1000	Novus biologics	NB110-53818
p62	rabbit	WB	1:1000	Novus biologics	NBP1-42821
		ICC	1:100		
		IHC	1:100		
LC3B	rabbit	WB	1:1000	Novus biologics	NB100-2220
		ICC	1:100		
		IHC	1:100		
LAMP-1	rabbit	WB	1:1000	Abcam	ab24170
		ICC	1:100		
		IHC	1:100		
TIMP-1	mouse	WB	1:750	SCBT	sc21734
	rabbit	ICC	1:100	Merck	AB770
		IHC	1:100		
CD63	mouse	WB	1:750	SCBT	sc5275
		ICC	1:100		
Aβ	rabbit	IHC	1:100	Abcam	ab201060
pULK1(S757)	rabbit	IHC	1:100	CST	6888s
PSD-95	rabbit	IHC	1:100	ThermoFisher Scientific	51-6900
		WB	1:1000		
SNAP-25	mouse	IHC	1:100	SCBT	sc20038
		WB	1:1000		
Synaptophysin1	mouse	WB	1:2000	Synaptic systems	101011
Homer1	mouse	WB	1:2000	Synaptic systems	160011
Actin	rabbit	WB	1:10000	Merck	A3854
GAPDH	rabbit	WB	1:1000	CST	2118S
phospho-Cofilin	rabbit	WB	1:500	CST	3311S
Cofilin	rabbit	WB	1:1000	CST	3318S

phospho-GSK3β (S9)	rabbit	WB	1:1000	CST	5558S
GSK3β	rabbit	WB	1:2000	CST	9315S
Pro-BDNF	mouse	WB	1:250	SCBT	sc65514
TrkB	mouse	WB	1:500	Abclonal	A21227
pERK1/2 (T202/Y204)	rabbit	WB	1:1000	CST	4377S
ERK2	rabbit	WB	1:1000	SCBT	sc153
pCREB (S133)	rabbit	WB	1:500	CST	9198S
CREB	rabbit	WB	1:500	CST	4820S
Anti-rabbit IgG-HRP inked	Goat	WB	1:4000	CST	7074S
Anti-mouse IgG-HRP inked	Horse	WB	1:4000	CST	7076S

Table: List of antibodies. WB=western blot, ICC=immunocytochemistry, IHC=immunohistochemistry, CST=Cell Signaling Technology, SCBT=SantaCruz Biotechnology

Primary Cortical Neuron Cultures:

Primary cortical neuron culture was performed following the method described earlier[7]. In short, the neocortex regions of E16-18 (sex not determined) of Sprague Dawley rat were dissected out under dissection microscope in serum free medium (DMEM/F12 [1:1]) supplemented with 6 mg/ml D-glucose, 100 μg/ml transferrin, 25 μg/ml insulin, 20 nM progesterone, 60 μM putrescine, 30 nM selenium) along with penstrep. Following gentle trituration, single cell suspension was seeded at 1.2 million in 2 ml per well of a previously PDL-coated 6-well tissue culture plate. After one day *in vitro* (1 DIV), media was changed with fresh Neurobasal media supplemented with B27. On 4 DIV, half of the used media was replaced with fresh neurobasal plus B27 media. Following six days of plating the neurons were treated as per experimental conditions in fresh neurobasal plus B27 media.

Preparation of oligomeric Aβ:

HFIP solvent (100%) was added to lyophilized $A\beta_{1-42}$ peptide to a final concentration of 1 mM and centrifuged in a speed vac (Eppendorf, Hamburg, Germany). The peptide pellet was re-suspended in DMSO at 5 mM concentration and sonicated in 37□C water bath for 10 min. The

peptide solution was aliquoted and stored at -80°C for later use. Before treatment, each aliquot was diluted in phosphate buffer saline (PBS: NaCl 137 mM, KCL 2.7 mM, Na_2HPO_4 10 mM, KH_2PO_4 2 mM, pH 7.4) and SDS (0.2%) to a concentration of 400 μM and incubated for 18-24 h at 37□C. Next, the suspension was further diluted with PBS to a final concentration of 100 μM and again incubated for 18-24 h at 37□C. The Aβ suspension was run in SDS-polyacrylamide gel electrophoresis (SDS-PAGE) followed by Sypro Ruby protein gel staining to check for oligomeric species.

Treatments on cells:

Cortical neurons were treated with either 1.5 μM Aβ or rat recombinant TIMP-1 peptide (R&D system, Minneapolis, USA) at 100 ng/ml[7] or a combination of both for 16 h as shown in figures.

Transfection studies:

Primary neuron cultures were introduced with Silencer Select siCD63 (s130868, Thermofisher Scientific, Waltham, MA, USA) or Silencer Select Negative control No. 1 siRNA (4390843, Thermofisher Scientific, Waltham, MA USA) on Day-4 following plating according to the manufacturer's protocol at 100 pmole/well (50 nM) of a 6-well tissue culture plate with the help of Lipofectamin 2000. Successful knockdown was verified following 72 h of incubation by western blot for CD63 in siCD63 transfected cells versus either Silencer Select Negative control No. 1 siRNA (data not shown) or untreated control cells. On Day-7 following plating, the cells were treated according to experimental paradigm.

Immunocytochemistry:

Neurons on PDL-coated glass cover slips were fixed in 4% PFA in PBS for 15-20 min at room temperature. Following PBS wash, the fixed cells were permeabilized and blocked with 3% goat serum in 0.3% Triton X-100 in PBS for 1-2 h. Next, cells were incubated with primary antibody overnight at 4˚C. Following the primary antibody incubation, cells were washed and incubated with specific species-matched secondary antibody tagged with Alexa fluor 546/488 for 1-2 h at room temperature. Nuclei staining were performed using Hoechst 33342 in PBS at 2 μg/ml for 30 min in dark. Cells were then mounted on glass slides using Prolong Gold antifade with DAPI. Images were taken in Leica Sp8 STED confocal microscope (Wetzlar, Germany) at specific

magnifications as mentioned in individual experiments. The fluorescence intensities for FOXO3a in the nucleus and whole cell were calculated separately by NIH-ImageJ software. Fluorescence intensity for FOXO3a in the cytoplasm was calculated by subtracting the nuclear FOXO3a from total cell FOXO3a. The ratio of nuclear FOXO3a to cytosolic FOXO3a under each condition is presented to indicate the translocation. In case of colocalization studies, Pearson's correlation coefficient was calculated from images taken at 60x magnification using Leica Sp8 software. Integrated density of staining, area of individual cell and the background fluorescence of individual image in different experimental conditions was derived using NIH-ImageJ software. The corrected total cell fluorescence (CTCF) was calculated as follows, CTCF = Integrated density – (area of selected cell x mean fluorescence of background readings).

Preparation of cell or tissue lysate:

Following treatment, cells were washed and scraped in PBS and harvested by centrifugation at 800 g at 4□C for 5 min. In case of tissues, cortex and hippocampus from mouse brain were micro-dissected, the tissue was immediately collected in RIPA buffer along with phosphastase inhibitor (Roche, Basel, Switzerland) and protease inhibitors mix (Takara Bio, Kusatsu, Japan). Alternatively in case of culture, cells were lysed by RIPA buffer (Sigma-Aldrich, St. Louis, USA) mixed with phosphastase inhibitor and protease inhibitor. For both tissue and cell pellet, each tube contents were sonicated by 2-3 pulses on ice to breakdown genetic material and incubated for 30 min on ice with intermittent vortexing. The lysed cells/tissue was then mixed with 5x sample buffer so that the final contents are at 1x sample buffer concentration. The protein concentration was estimated by Lowry method.

Western blotting:

Fifty µg of protein from each treatment condition was run in SDS-PAGE. The resolved proteins were then transferred to PVDF membrane. The membrane was next blocked with 5% BSA for 1 h at room temperature, following which the membranes were incubated with primary antibodies overnight at 4□C. Membranes were washed with TBST [1.5 M NaCl, 1 M Tris (pH 7.5), 0.1% Tween20] followed by incubation with HRP-conjugated suitable secondary antibody for 1 h at room temperature. Three more TBST washes were given to remove unbound antibodies. Protein bands were detected on ChemiDoc MP imaging system (Bio-Rad laboratories, California, USA)

using ECL reagents. Densitometric quantification of each band was done by NIH ImageJ software (NIH, Bethesda, MD, USA), normalized with loading control (either Actin or GAPDH as mentioned) and fold change was compared with the untreated control.

Animal housing and care:

Male C57BL6 (wild-type or WT) or 5xFAD mice were housed maximum six per cage in standard individually ventilated cages (IVC) with proper bedding material. Mice were maintained by trained caretakers, checked daily and kept in a temperature-controlled room (24 ± 2°C), with 12 to 12 h light-dark cycle, humidity (60 ± 5%) and access to food and water ad libitum in the animal house of CSIR-Indian Institute of Chemical Biology, Kolkata. For age-wise comparisons, 5xFAD mice of different ages as defined later were procured along with age-matched WT mice. For all other animal experiments, 6-month-old 5xFAD and age-matched WT mice from different litter groups were used for treatment. All the studies were conducted in accordance with the guidelines formulated by the Committee for the Purpose of Control and Supervision of Experiments on Animals (Department of Animal Husbandry and Dairying, Ministry of Fisheries, Animal Husbandry and Dairying, Govt. Of India), with approval from the Institutional Animal Ethics Committee (IAEC) on the required care and use of animals in laboratory research.

Stereotaxic procedures:

For mouse, a combination of ketamine (100 mg/kg i.p.) and xylazine (10 mg/kg i.p.) in 0.9% normal saline was used for anesthetization (i.p.) for a short duration for stereotaxic surgery. Individual mouse was placed in a suitable stereotaxic frame (Stoelting, MO, USA) with the incision bar initially positioned at the Bregma point. The body temperature of the animal was maintained at 37°C using a homeothermic blanket (Harvard apparatus, MA, USA). Recombinant TIMP-1 (5 ng) diluted in artificial cerebro spinal fluid (aCSF) in a total volume of 5 µl was injected intracerebroventricularly (i.c.v.) into the ventricle (lateral, 0 cm from the bregma; anteroposterior, -1.6 mm from bregma; dorsoventral, -2.2 mm from bregma). The flow rate was kept at 0.5 µl/min using a worker bee syringe pump (BAS, West Lafayette, USA). The peptide solution was allowed to diffuse for an additional 10 min following actual injection duration to prevent backflow.

Behavioral assessments:

The experimental mice were randomly divided into four groups – WT, 5xFAD, 5xFAD+aCSF, 5xFAD+TIMP-1 (5 ng). Behavioral tests were started on Day-8 following TIMP-1 infusion.

Open-field test (OFT)

Open-field test (OFT) apparatus (IR Actimeter, Panlab, Barcelona, Spain) consists of open field Plexiglas arena with photocell emitters and receptors positioned at equal distance along the perimeter of the arena (278×236×300 mm). These emitters and receptors create an x-y grid of invisible infrared rays. Mouse moving across the arena makes beam breaks that were recorded for 10 min and the animal trajectories were analyzed by the ActiTrack software (Panlab, Barcelona, Spain). The arena was divided into two zones; a square area occupying one-third of the total arena area in the center was considered as the 'Inner zone' and the rest the 'Outer zone'. The total distance travelled (cm), the speed of the mouse (cm/sec) and the time spent in the outer zone (periphery) and that in the inner zone (center) in seconds were recorded, where the latter is generally utilized to measure anxiety.

Elevated plus maze (EPM) test

EPM test for long-term memory was carried out according to the standard protocol as described earlier[7]. Briefly, in the two-day test, on day one the animal was placed at the edge of one of the open arms of plus maze with its face away from the center for exploration for 5 min. On day two, the mouse was placed similarly on to the open arm for 5 min. The transfer latency to the closed arm on day one was recorded as initial transfer latency (ITL) and on day two was recorded as retention transfer latency (RTL).

Novel Object Recognition (NOR) test

In this two-day test for hippocampus-dependent recognition memory, a mouse was allowed to explore a rectangular box (50 cm x 30 cm) with two identical (color and dimensions) objects placed at parallel corners for 5 min on Day-1. On Day-2, one of the objects was replaced with an object of different color and shape and the mouse was returned to the box for 5 min. The time the mouse spent with each of the two objects on Day-2 were noted and presented as exploration time (sec). Discrimination index (DI) and preference index (PI) were derived according to the

formulas – DI = (TN-TF)/(TN+TF), PI = TN/(TN+TF)*100 from the Day-2 data where TF is time spent with the familiar object and TN is time spent with the novel object.

Fear Conditioning Test

Fear conditioning tests are routinely utilized to study long-term associative learning processes involving amygdala, hippocampus and specific parts of cortex. Each mouse was placed in a sound-attenuating chamber with a stainless-steel grid floor that delivers a foot-shock (Panlab, Barcelona, Spain) and is connected to a recorder that records the freezing behavior. Rodents express their fear towards an aversive stimulus with a complete loss of movement except for breathing termed 'freezing'. Animals were handled once per day for three days and habituated in the experimentation room before the start of the actual experiment. Only one animal was allowed in the experimentation room at a time. Both context-dependent and cue-dependent fear conditioning tests were performed as described earlier[7] with modifications as mentioned below.

Contextual fear conditioning test

On the day of training, the animal was placed in the chamber and allowed to acclimatize for a 2 min period. After acclimatization, the mouse was exposed to four sessions of an unconditional stimulus (each session- 89 sec pre-shock interval; 0.4 mA, 1 sec foot-shock) co-terminating with a 2 min period without stimuli (10 min total). Context dependent fear memory retention was tested on day two when the mouse was returned to the same environment but this time without foot-shock. Freezing behavior was calculated by PACKWIN 2.0 software (Panlab, Barcelona, Spain) during an 8 min run time.

Cue-dependent fear conditioning test

On the day of training, each mouse was initially exposed to the chamber for a 2 min period for acclimatization. Next, four 29-sec sessions of light and sound (80 dB, 2500 Hz) cues co-terminating with a foot shock (0.4 mA, 1 sec for mouse) were delivered with an inter-trial interval of 1 min, following which the mouse was given 2 min of rest (10 min in total) before it was removed from the chamber. On day two, the context of the chamber was altered by attaching white sheets to the chamber walls and the floor and the mouse was returned to this new environment with same sessions of cues but without foot-shock. Cue-dependent fear memory

retention was assessed by recording freezing behavior during the 8 min test period by PACKWIN 2.0 software (Panlab, Barcelona, Spain).

Immunohistochemistry:

After 14 days of TIMP-1 infusion, each mouse was transcardially perfused under anesthesia with urethane [1g/kg body weight (MP Biomedicals, lllkirch, France) in 0.9 % NaCl solution (i.p.)] with chilled 100 mM PBS (pH 7.4). Perfusion was continued with 4% (w/v) PFA solution in PBS, following which the mouse was decapitated and the brain was isolated in chilled 4% PFA solution for overnight fixation at 4°C and then transferred in 30% (w/v) sucrose solution in PBS for cryopreservation at 4°C. Coronal sections (20 µm thick) were obtained using a cryotome (Thermo Shandon, Pittsburg, USA) and collected on to gelatine-coated slides for immunohistological staining. Selected brain sections were washed with PBS thrice followed by permeabilization with PBS + 0.4% Triton-X for 40 min. Next, the sections were washed with PBS + 0.1% Triton-X (PBST) three times, 5 min each. The sections were then blocked with 4% BSA in PBST for 1 h. Following blocking, the sections were incubated with primary antibodies diluted in the blocking solution for 48 h at 4°C. Next, PBST washes were given to the tissue slices to remove unbound antibodies and incubated with appropriate Alexa fluor-tagged secondary antibodies diluted in the blocking solution at RT for 2 h. Afterwards, sections were again washed in PBST and incubated with Hoechst 33342 in PBS at 2 µg/ml for 30 min at 37°C. Further PBS washes were given to the sections and mounted with Prolong Gold Antifade with DAPI reagent on to glass slides for microscopic analysis in Leica Sp8 STED confocal microscope (Wetzlar, Germany).

$A\beta_{1-42}$ plaques were evaluated by calculating the percentage of plaque area and plaque number by ImageJ software from 40x images of the hippocampus taken in Leica Sp8 STED confocal microscope (Wetzlar, Germany). For SNAP25, PSD95, pULK1, p62, LC3B and LAMP1, CTCF = Integrated density – (area of selected cell x mean fluorescence of background readings) was calculated from cells in the cortices and hippocampi of mouse brain sections with ImageJ software from 40x images taken in Leica Sp8 STED confocal microscope (Wetzlar, Germany). TIMP-1 count denotes the number of TIMP-1 antibody-stained puncta in the hippocampal-cortical regions from 20x images of mouse brain sections taken under confocal microscope. The number of pH2Ax positive nuclei of total number of nuclei in the specific area was counted by

ImageJ software from 100x images taken in the hippocampal and cortical regions by confocal microscope and the percentage was calculated.

Terminal deoxynucleotidyl transferase dUTP nick end labeling (TUNEL) assay:

TUNEL assay was performed to detect apoptotic cell death using Clonetech ApoAlert DNA Fragmentation kit (Takara, Kusatsu, Shiga, Japan) according to the manufacturer's protocol. Fixed tissue sections were hydrated with PBS and incubated with Proteinase K solution (20 µg/ml, diluted from the stock provided in the kit) for 20 min. The reaction was terminated by washing with PBS, followed by addition of 4% PFA in PBS to the sections. Following PBS washes, tissue sections were equilibrated in the Equilibriation buffer at RT for 10 min. The slices were then incubated in a solution of nucleotide mix and Tdt enzyme for 1 h at 37°C in dark. The tailing reaction was stopped by addition of 2XSSC buffer (provided in kit) at RT for 15 min. Next, the sections were rinsed again in PBS and incubated with Hoechst solution for 30 min at 37°C, washed with PBS and mounted with Prolong Gold Antifade with DAPI for microscopic analysis. The percentage of apoptotic cells were calculated by dividing the number of TUNEL-positive cells with the total number of cells (Hoechst-stained nuclei) multiplied by 100.

Isolation of synaptosomes:

Synaptosomes were isolated from adult mouse brain by the method described earlier with some modifications[29], 14 days following TIMP-1 infusion. Briefly, the freshly dissected mouse brain tissue (hippocampus or cortex), pooled from six to seven mice per experimental group, was homogenized in an isotonic sucrose gradient buffer (diluted to 1x from a stock of 4x Gradient buffer - 1.28 M sucrose, 4 mM EDTA, 20 mM Tris, pH 7.4). The homogenate was then centrifuged at 1000g for 10 min at 4°C to separate supernatant and debris. The supernatant was loaded onto a discontinuous Percoll gradient composed of three layers – 3% (vol/vol), 10% (vol/vol) and 23% (vol/vol) percoll. The gradient was then centrifuged at 31,000 g for 5 min at 4°C (excluding acceleration and deceleration time). The synaptosomes separate as a layer between 10% and 23% percoll layers. The synaptosome layer was collected, diluted in aCSF and centrifuged to remove percoll contamination. The final synaptosomal pellets were re-suspended in 1x sample buffer before protein estimation for SDS-PAGE run. Alternatively, for determination of Fibrillar/Globular (F/G) actin content ratio, the synaptosomal pellet was further fractionated into the cytoskeleton and cytoplasmic fractions. Accordingly, the synaptosomal

pellet was resuspended in a Mg^{2+}-containing buffer (50 mM Tris, 2 mM $MgCl_2$, pH 7.4) and vortexed while maintaining the suspension on ice. Next, TritonX-100 was added to the suspension at a final concentration of 0.5% and kept on ice for 20-30 min. Then, it was allowed to centrifuge at 12,000 g for 10 min at 4^oC. The pellet thus obtained is the cytoskeleton (CSK) fraction containing F actin while the supernatant (SUP) contains all the cytosolic proteins including G actin. Each of the fractions was resuspended in 1x sample buffer for western blot analysis.

Golgi-cox impregnation and staining procedure:

Golgi-cox staining was performed according to the protocol described previously[71]. Fourteen days following TIMP-1 infusion, the brain of the mouse was taken out and immediately submerged in the impregnation solution - a mixture of five parts by volume of Solution A (5% potassium dichromate in distilled water (DW)), five parts by volume of Solution B (5% mercuric chloride in DW), four parts by volume of Solution C (5% potassium chromate in DW) and ten parts by volume of DW, and kept in dark at RT. The solution was changed after 24 h with fresh impregnation solution and incubated for two weeks. Next, the brain was transferred to Solution D, a cryoprotectant solution prepared by mixing 20 g of sucrose and 15 ml glycerol in 100 ml of DW and kept at 4^oC in dark for 24 h following which fresh cryoprotectant solution was added. A period of 2-3 days was given for the brain to sink to the bottom. Sectioning was done at -25^oC in a cryotome (Thermo Fisher Scientific, MA, USA) and 100 µm thick slices were collected on gelatine-coated glass slides. The sections were allowed to dry for some time, washed twice with DW and stained with 20% ammonium solution for 10 min in dark. Following two more washes with DW, sections were dehydrated through 50%, 70%, 95% and 100% (twice) ethanol for 5 min in each. The sections were removed off fat by xyline wash, twice for 5 min each. The sections were mounted in DPX reagent, covered with a coverslip and allowed to dry at room temperature for 3-4 days in dark before bright-field imaging in Leica Sp8 STED confocal microscope (Wetzlar, Germany). For measuring spine density, distal dendrites with similar diameters were imaged in the cortex or stratum radiatum of the CA1 hippocampus, magnified in Adobe Photoshop (San Jose, California, USA) and counted spines on printed copies. Any small protrusion on a dendrite was considered a spine. Spine density was calculated from many distal dendrites amounting for a total length of 1200-2000 µm (40-80 dendritic stretches) per experimental group.

Electrophysiology:

Fourteen days following TIMP-1 injection, mice were anesthetized in a 5% gaseous isoflurane chamber (Aerrane, Baxter Healthcare Corporation; Fluovac, Harvard Apparatus, USA) and perfused transcardially at a speed of 45 ml/min using a peristaltic pump (Cole Parmer, USA) with cold (7-8°C) aCSF [NaCl (118 mM), KCl (2.5 mM), NaH_2PO_4 (1.5 mM), $NaHCO_3$ (25 mM), $C_6H_{12}O_6$ (25 mM), $MgCl_2$ (1.3 mM) and $CaCl_2$ (2.2 mM), adjusted to a pH of 7.4 with an osmolarity of 310-320 mOsm/L] which was continuously bubbled with carbogen (5% CO_2 and 95% O_2, Chemix Special Gases and Equipments, India). The brain was immediately shelled out of the skull and submerged in ice-cold carbogenated aCSF. The hemispheres were separated and 400µm thick para-sagittal slices were taken using a vibratome (Leica VT, 1200S, Leica Biosystems, Germany) with a blade speed of 0.14 mm/s and amplitude 1.20 mm. The slices were transferred and kept in a brain slice keeper (BSK4-Quad, Automate Scientific Inc CA, USA) in carbogenatedaCSF at RT. For extracellular Field Excitatory Postsynaptic Potential (fEPSP) recordings, after 2 h incubation at RT, slices were transferred to a recording chamber (Warner instruments, USA), perfused continuously with carbogen-bubbled aCSF at RT with the help of a Minipuls Evolution peristaltic pump (Gilson Inc USA). The flow rate was maintained at 2 ml/min. Under observation in a stereozoom microscope (Olympus, Japan), Platinum-iridium cluster bipolar electrodes (Frederick Haer Company Inc, ME, USA) were placed to stimulate Schaffer collaterals that synapse with CA1pyramidal neurons. Borosilicate glass microelectrode (Sutter instruments, USA) filled with 2M NaCl was used as the recording electrode and was placed in the stratum radiatum layer of the CA1 region of dorsal hippocampus, and recordings were obtained under immersed conditions. fEPSPs were induced by injecting 0.1-ms width square wave pulses using a stimulus isolator in a constant current mode that produced fEPSP with a typical stimulus artefact, fibre volley and a negative deflection. fEPSPs were induced at a test stimulus frequency of 0.033Hz during the whole experimental duration. A stable baseline of minimum 20 min was recorded before proceeding with the evaluation of other parameters. The studies conducted sequentially wereas follows:

(i) **Input-output (I-O) relationship** was measured by increasing the input current strength (by 20 µA increment) until population spike was observed. The stimulus current strength for the test was kept at a value that evoked a 40% of the maximum fEPSP slope value.

(ii) **Paired-pulse facilitation (PPF)** was determined by supplying two pulses in close succession with inter-stimulus intervals (ISI) ranging from 30-300 ms with an increment of 30 ms. Paired-pulse ratio (PPR) was calculated by dividing the slope of fEPSP2 by fEPSP1.

(iii) Following 20 min of baseline recording, **post-tetanic potentiation** (PTP), **short-term potentiation** (STP) and **long-term potentiation** (LTP) were evoked using single theta burst stimulation (TBS, 4 pulses/burst at 100 Hz, 20 bursts with 200-ms interval). Recordings were carried out up to 60 min following TBS induction. Only slices that displayed stable responses for a minimum of 60 min post TBS were considered for analysis of PTP, STP and LTP. The average slopes of fEPSPs normalized to baseline measured for the first 3 min (PTP), from 21st-30th min (for STP) and 41st-60th min (for LTP) post TBS were used for statistical comparisons.

The fEPSP responses were amplified using a differential amplifier (A-M systems, USA) and digitized with the help of a digitizer (National Instruments, USA). A noise eliminator (Humbug, Quest scientific) was utilized to eliminate the effect of electrical interference on the recordings. The data were acquired and analyzed using WinLTP® v2.3 software (WinLTP Ltd, UK).

Statistical Analysis:

All data were analyzed and graphs were created by using Prism software (v8.4.2 (679), GraphPad Inc, USA). For analysis of significant difference between only two groups two-tailed unpaired student's t-test was used. For comparing more than two experimental groups, one way ANOVA analysis followed by Tukey's multiple comparison post hoc test was used in all the experiments except stated otherwise. However, in case of the input-output curve and PPF curve, two-way ANOVA followed by Tukey's multiple comparison post hoc analysis was used to calculate the effect of TIMP-1. All data are presented as mean ± standard error of mean (s.e.m.), and $P<0.05$ was considered to be statistically significant.

ACKNOWLEDGEMENTS

We, the authors, would like to thank Dr. P. K. Sarkar for critical reading of this manuscript and helpful discussions. We would like to thank Sammani Sarkar for her help in preparing the

artwork of the manuscript. We would also like to extend our gratitude towards Mr. Sounak Bhattacharya for his technical assistance in confocal microscopy. The work was supported in part by one of the 12th Five Year Plan Projects, miND (BSC0115) of CSIR, Govt. of India and by the Department of Biotechnology, Govt. of India, Project BT/PR14383/MED/12/475/2010.

AUTHOR CONTRIBUTIONS

Conceptualization, S.S. and S.C.B.; Methodology, S.S., K.G. and R.K.P.; Validation, S.S. and K.G.; Formal analysis, S.S. and K.G.; Investigation, S.S., K.G. and R.K.P., Writing – Original Draft, S.S.; Writing – Review and Editing, S.C.B., K.G. and B.N.S.; Visualization, S.S. and S.C.B.; Funding acquisition, S.C.B.; Resources, S.C.B. and B.N.S.; Supervision, S.C.B. and B.N.S.

FIGURE TITLES AND LEGENDS

Figure 1: Exogenous TIMP-1 injection corrects cognitive deficits in 5xFAD mice. A, Representative immunoblots showing endogenous TIMP-1 levels in wild type (WT) and 5xFAD mice in the hippocampus at 2 months (M), 4M, 6M and 8M of age (also refer Figures S1A and S1B). **B**, Quantification of TIMP-1 levels were normalized to actin. Relative expression was calculated w.r.t. WT in each age group (N=6 mice/group; two-tailed unpaired t-test, mean±s.e.m.). **C**, Schematic of stereotactic injection of TIMP-1 (5 ng) and subsequent behavioral experiment schedule. **D**, Representative immunofluorescence images of coronal sections showing hippocampal regions from 5xFAD and 5xFAD+TIMP-1 mouse brains stained for TIMP-1 (green) and nuclei (blue) on Day-8 post TIMP-1 injection; scale bar-50 µm. **E**, Quantification for TIMP-1 immunoreactivity in the hippocampus shown as TIMP-1 puncta count (N=3 mice/group, analyzed 3 slices/mouse brain; two-tailed unpaired t-test, mean±s.e.m.). **F-R**, Battery of behavioral tests were performed with four groups of mice – WT, 5xFAD, 5xFAD+aCSF and 5xFAD+TIMP-1 starting on Day-8 following intracerebroventricular TIMP-1 injection to check for cognitive functions. **F**, Representative infra-red images of the path travelled by a mouse in each group in Open-field test (OFT). **G**, Average total distance travelled (cm) in the whole open arena and **H**, Average time spent (sec) in the outer zone of the arena in 10 min of OFT. One-way ANOVA, Tukey's post hoc, mean±s.e.m. **I**, Experimental set-up for elevated-plus maze (EPM) test. **J**, Average latency (sec) of mouse to the closed arm of EPM recorded on Day-1 as initial transfer latency (ITL) and on Day-2 as retention transfer latency (RTL) and their difference (ITL-RTL). For ITL versus RTL within each group, two-tailed unpaired t-test, mean±s.e.m; @P<0.0001, #P<0.001. For comparison of ITL-RTL among groups, One-way ANOVA, Tukey's post hoc, mean±s.e.m. **K**, Experimental set-up for Day-2 of Novel object recognition (NOR) test with one novel (*N*) and one familiar (*F*) object for **L-N**. **L**, Average exploration time (sec) with *F* versus *N* objects within 5 min on Day-2 of NOR; two-

tailed unpaired t-test, mean±s.e.m. **M**, Discrimination index and **N**, Preference index (%) calculated among groups from Day-2 data of NOR, One-way ANOVA, Tukey's post hoc, mean±s.e.m. For OFT, EPM and NOR also see Figure S2. **O**, Experimental set-up for Day-1 of contextual fear conditioning (CFC) test. **P**, Percentage freezing of mice on Day-2 of CFC. **Q**, Experimental set-up for Day-1 of Cue-dependent fear conditioning (CDFC) test and **R**, Percentage freezing of mice on Day-2 of CDFC, One-way ANOVA, Tukey's post hoc, mean±s.e.m. for **P** and **R**. *P<0.05, **P<0.01, ***P<0.001 and ****P<0.0001; ns, not significant. Each point of the Scatter plots with bar represents one animal. Number of animals and exact P values in each test are given in Supplementary Table-1.

Figure 2: TIMP-1 binds to CD63 on neurons and improves Akt phosphorylation. A, Schema showing TIMP-1 binding to CD63 receptor activates PI3K/Akt pathway. **B**, Representative immunofluorescence images for CD63 (green) and TIMP-1 (red) in primary cortical neurons 16h post treatment with or without (CON) TIMP-1 (100 ng/ml). Merged panel shows colocalization (yellow) between the two proteins scale bar, 10µm. **C**, Colocalization analysis by calculating Pearson correlation coefficient between TIMP-1 and CD63 (N = 6 independent experiments; two-tailed unpaired t-test, mean±s.e.m; ****P<0.0001). **D**, Schema for primary neuron culture and treatment. **E**, Representative immunoblot for CD63 from primary cortical neurons treated with or without siCD63 for siRNA validation. **F**, Densitometric analysis and calculation of CD63fold change w.r.t. CON utilizing Actin for loading control normalization (N = 6 independent experiments; two-tailed unpaired t-test, mean±s.e.m; *P<0.0001). **G**, Representative immunoblots for pAkt(S473), corresponding Akt and Actin from primary neurons, with or without CD63 downregulation, treated with or without Aβ (1.5 µM), TIMP-1 or co-treated with Aβ+TIMP-1. **H**, Densitometric analysis and calculation of fold change of pAkt(S473)/Akt w.r.t. CON for N = 6 independent experiments; two-tailed unpaired t-test, mean±s.e.m.*P=0.0109, $^{\#}$P=0.0499, and $^{@}$P=0.0114.

Figure 3: TIMP-1 protects primary cortical neurons against apoptosis. **A**, Schema showing that Aβ treatment to neurons causes Akt dephosphorylation at S473 and downstream nuclear translocation of FOXO3a upregulating apoptosis as previously reported[23,24]. **B**, Representative immunoblots for pFOXO3a(S253) and corresponding total FOXO3a and Actin at 16 h post treatment with or without TIMP-1 (100 ng/ml) in presence or absence of Aβ(1.5 µM) in primary cortical neurons. **C**, Densitometric analysis followed by calculation of fold change for pFOXO3a/FOXO3aw.r.t. control (CON) (N = 4 independent experiments; One-way ANOVA, Tukey's post hoc, mean±s.e.m.). **D**, Representative merged immunofluorescence images for FOXO3a (green) and nuclei stained with Hoechst (blue). White arrows indicate green dots for FOXO3a in the nuclei in the Aβ-treated neurons. **E**, Quantification of nuclear translocation of FOXO3a by ImageJ, N = 3 independent experiments, 20 cells/experiment; One-way ANOVA, Tukey's post hoc, mean±s.e.m. **F**, Representative panel of immunoblots from primary neuron lysates probed with pro- and anti-apoptotic proteins as indicated along with the corresponding loading control or actin from the same blot. **G-M**, Densitometric analyses followed by

calculation of fold change w.r.t. CON for BIM (**G**), PUMA (**H**), Bcl-2 (**I**), Bcl-xL (**J**), BAX (**K**), pH2Ax (**L**) and cCas3 (**M**), (N = 3 independent experiments; One-way ANOVA, Tukey's post hoc, mean±s.e.m.).*P<0.05, **P<0.01, ***P<0.001, ****P<0.0001. cCas3, cleaved Caspase 3. Also see Figure S4.

Figure 4: TIMP-1 addition ameliorates autophagy flux in Aβ-treated neurons. A, Schematic showing Aβ-induced Akt inactivation causes impaired autophagy flux in neurons[27]. **B**, Representative immunoblot for ATG5-ATG12 complex along with corresponding actin from primary neurons at 16 h post treatment with or without TIMP-1 (100 ng/ml) in presence or absence of Aβ (1.5 µM). **C**, Densitometric analysis and calculation of fold change in ATG5-ATG12, normalized to actin, w.r.t. control cells (CON), (N = 3 independent experiments; One-way ANOVA, Tukey's post hoc, mean±s.e.m.). **D-I**, Representative immunoblots and corresponding fold changes w.r.t. CON for p62 (**D-E**), LC3B-II (**F-G**) and LAMP1 (**H-I**). N = 4 independent experiments; One-way ANOVA, Tukey's post hoc, mean±s.e.m.*p<0.05, **p<0.01, ***p<0.001 for **B-I**. **J,L,N**, Representative merged immunofluorescence images for p62 (**J**, red), LC3B (**L**, green) and LAMP1 (**N**, green) in primary neurons treated similarly as in western blot, at 16 h post treatment; nuclei visualized with Hoechst (blue); scale bar, 10 µm. A zoom-in panel is shown for each protein to highlight the change in fluorescence intensities within individual cell. Corrected total cell fluorescence (CTCF) calculated for p62 (**K**), LC3B (**M**) and LAMP1 (**O**) from N = 3 independent experiments, analyzed 90-150 cells/treatment condition; One-way ANOVA, Tukey's post hoc, mean±s.e.m; *P<0.0001 versus CON,#P<0.0001 versus Aβ. Also see Figure S5.

Figure 5: TIMP-1 improves synaptic protein expressions in 5xFAD mice. A, Schematic showing methodology for whole tissue and synaptosome isolation from hippocampus (Hpc) and cortex (Ctx) of mouse brain. **B, D,** Representative immunofluorescence images for SNAP25 (green, **B**) and PSD95 (red, **D**) in coronal sections of WT, 5xFAD and 5xFAD+TIMP-1 hippocampus; scale bar, 30 µm at 40x magnification (white box indicates the region selected for further zoom-in). Zoom-in merged images are shown with nuclei stained with Hoechst (blue); scale bar, 15 µm. CTCF calculated for SNAP25 (**C**) and PSD95 (**E**), N= 3 animals/group, n = 50 cells/animal from Hpc quantified from 40x images; One-way ANOVA, Tukey's post hoc, mean±s.e.m. *P<0.0001, #P<0.0001 for **C** and **E**. Refer Figures S6A-S6D for cortical expressions of the above two proteins. Representative immunoblots for SNAP25 (**F**) and PSD95 (**H**) from Hpc whole tissue lysates collected 14 days post TIMP-1 injection. Densitometric analyses and fold changes for normalized SNAP25 (**G**) and PSD95 (**I**) w.r.t. to WT group. N = 4 animals/group; One-way ANOVA, Tukey's post hoc, mean±s.e.m. **G**, *P=0.0449, #P=0.0011; **I**, *P=0.012, #P=0.0351. Also see Figures S6E-S6F for HOMER-1 and Synaptophysin-I (SYNAP) expressions in whole Hpc. **J**, Representative immunoblots for synaptic proteins from synaptosomes isolated separately from Ctx and Hpc. Densitometric analyses and fold changes w.r.t. WT were calculated for pre-synaptic markers SNAP25 (**K**, Ctx *P=0.0012, #P=0.0001; Hpc, *P=0.0049, #P=0.0154) and SYNAP (**L**, Ctx, *P=0.0354; Hpc, *P=0.003), and post-

synaptic markers - PSD95 (**M**, Ctx *P=0.0007, #P=0.0397; Hpc, *P=0.0008, #P=0.0260) and HOMER-1 (**N**, Ctx *P<0.0001, #P=0.0081; Hpc, *P=0.0024). N = 3-5 independent synaptosome isolations/group, 6-7 pooled animals/synaptosome isolation/group; mean±s.e.m. Statistical tests used for **K-N** are given in Supplementary Table 1.

Figure 6: TIMP-1 improves spine density and size in 5xFAD mouse. A, Representative coronal section of a mouse brain showing the CA1 region of hippocampus (Hpc, red box) and the cortex (Ctx, yellow box) targeted for spine density calculation following Golgi-cox staining (scale bar-100 µm). **B**, Representative images of dendritic segment showing spines in Hpc (upper panel) and Ctx (lower panel) from the four treatment groups, 14 days post TIMP-1 injection; scale bar, 2 µm. **C-D**, Quantification of the number of spines/10µm from Hpc (**C**, *P<0.0001 versus WT; #P<0.0001 versus 5xFAD) and Ctx (**D**, *P<0.0001 versus WT, #P<0.0001 versus 5xFAD). N =3 animals/group, 40-80 dendritic stretches/group foreach brain region; One-way ANOVA, Tukey's post hoc, mean±s.e.m. **E**, Schema for synaptosome isolation followed by fractionation for cytoskeleton (CSK) and cytoplasmic/supernatant (SUP) fractions. **F**, Representative immunoblots for filamentous (F, in CSK fraction) actin and globular (G, in SUP fraction) actin from Hpc and Ctx synaptosomes. **G-H**, Densitometric analysis and fold change for F/G actin content w.r.t. WT from Hpc (**G**, *P=0.0038, #P=0.0101) and Ctx (**H**, ns=not significant). N=4 independent synaptosome isolations/group, 6-7 pooled animals/synaptosome isolation/group; One-way ANOVA, Tukey's post hoc, mean±s.e.m. **I**, Representative immunoblots for pCofilin(S3) and Cofilin from Hpc and Ctx synaptosomes. **J-K**, Densitometric analysis and fold change for pCofilin/Cofilin from Hpc (**J**, *P=0.0125, #P=0.0002) and Ctx (**K**, *P=0.0313, #P=0.0127). N=4 independent synaptosome isolations/group, 6-7 pooled animals/synaptosome isolation/group; One-way ANOVA, Tukey's post hoc, mean±s.e.m.

Figure 7. BDNF and related signaling pathways are induced by TIMP-1 treatment to 5xFAD mice. A-L, Western blot (WB) data from Whole hippocampal (Hpc) tissue lysates 14 days post TIMP-1 treatment. Representative immunoblots for Pro-BDNF (**A**), TrkB (**C**), pAkt(S473) (**F**), pAkt(T308) (**H**) and pERK1/2 (**J**) with corresponding loading controls. Densitometric analyses and normalized fold change w.r.t. WT for Pro-BDNF (**B**), fl-TrkB (**D**), t-TrkB (**E**), pAkt(S473)/Akt (**G**), pAkt(T308)/Akt (**I**), pERK1/ERK2 (**K**) and pERK2/ERK2 (**L**). N = 3-4 mice/group; One-way ANOVA, Tukey's post hoc, mean±s.e.m. **M-X,** WB data from Hpc synaptosomes 14 days post TIMP-1 treatment. Representative blots for Pro-BDNF (**M**), TrkB (**O**), pAkt(S473) (**R**), pAkt(T308) (**T**) and pERK1/2 (**V**) with corresponding loading controls. Densitometric analyses and normalized fold change w.r.t. WT for Pro-BDNF (**N**), fl-TrkB (**P**), t-TrkB (**Q**), pAkt(S473)/Akt (**S**), pAkt(t308)/Akt (**U**), pERK1/ERK2 (**W**) and pERK2/ERK2 (**X**). N=7 independent synaptosome isolations/group, Mixed effect analysis, Tukey's post hoc for **N**; N=4-6 independent synaptosome isolations/group, One-way ANOVA, Tukey's post hoc for **P,Q,S,U,W,X**. Each synaptosome isolation (N) pooled from 6-7 animals for each group. All data expressed as mean±s.e.m. fl-TrkB, Full-length TrkB; t-TrkB, truncated TrkB. Also see Figure S8 for WB results from cortical synaptosomes. *P<0.05 versus WT,

$^{\#}$P<0.05 versus 5xFAD, ns=not significant. Exact P values for this figure are given in Supplementary Table 1.

Figure 8: Deregulated basal synaptic transmission and long-term potentiation at Schaffer collateral-CA1 synapses in 5xFAD mouse are enhanced by TIMP-1 through inhibition of hippocampal GSK3β activity but paired pulse facilitation ratio remains unaffected in all the groups. A, Schema showing regions of the hippocampus – CA1, CA2, CA3 and Dentate gyrus (DG) and the Entorhinal cortex (EC). The dotted lines mark the connecting fibres – Schaffer collateral (SC), Mossy fibres (MF), Perforant pathway (PP), Associational commissural fibres (AC). Stratum radiatum (SR) is where the recording electrode is placed in the CA1 region. **B**, Representative field excitatory post-synaptic potentiation (fEPSP) traces of slices from WT, 5xFAD, WT+TIMP- and 5xFAD+TIMP-1 mice treatment groups with increasing current stimulus strength (20 – 300 µA with 20 µA increments). **C**, Input-output (I-O) relationship (fEPSP slopes along a step-wise rise in stimulus intensity) representative of the mean fEPSP value of all the slices in each group at each stimulus current strength from 20 – 300 µA (n=9-15 slices/group, N=5-6 mice/group, Two-way ANOVA, mean±s.e.m.; *P<0.05, $^{\#}$P<0.05. **D**, Area under curve (AUC) from **C**, One-way ANOVA, Tukey's post hoc, mean±s.e.m. *P=0.0153, $^{\#}$P=0.0103. **E**, Paired-pulse facilitation (PPF) ratio along increasing inter-stimulus interval (30 to 300 ms with 30 ms increments), Two-way ANOVA, mean±s.e.m. **F**, AUC from **E**, n=9-15 slices/group, N=5-6 mice/group, One-way ANOVA, Tukey's post hoc, mean±s.e.m. **G**, Time course of fEPSP responses with 20 min pre-TBS and 60 min post-TBS. Note the time segments post-TBS demarcated for calculating post-tetanic potentiation (PTP), short-term potentiation (STP) and long-term potentiation (LTP). **H**, Representative fEPSP tracings of slices from the four groups. Solid line represents pre-TBS response (baseline) and dotted line represents post-TBS response. Note the decrease in the magnitude of LTP in 5xFAD (pink) compared to WT (grey) and increase in LTP in 5xFAD+TIMP-1 (green) group compared to 5xFAD. **I**, AUC from **G,** One-way ANOVA, Tukey's post hoc, mean±s.e.m. *P= 0.0088, $^{\#}$P= 0.0207. **J-L**, Bar graphs for PTP (3 min post-TBS) (**J**), STP (21st-30th min) post-TBS (**K**), LTP (41st-60th min post-TBS) (**L**); n= 9-12 slices/group, N=5-6 mice/group, One-way ANOVA, Tukey's post hoc, mean±s.e.m.*P=0.0165, $^{\#}$P=0.0355. **M**, Representative immunoblots for pGSK3β(S9) from whole tissue and synaptosomal lysates from hippocampus (Hpc), 14 days following TIMP-1 injection. **N-O**, Densitometric analysis and fold change w.r.t. WT for pGSK3β/GSK3β from whole tissue (**N**, *P=0.0003, $^{\#}$P=0.0017) and synaptosome (**O**, *P=0.0202, $^{\#}$P=0.0094). N=3 mice/group for **N**, N=4 independent synaptosomal isolations for **O**; One-way ANOVA, Tukey's post hoc, mean±s.e.m. *P versus WT, $^{\#}$P versus 5xFAD for **C-D,I,L,N-O**. ns=not significant.

SUPPLEMENTARY INFORMATION

Figure S1. TIMP-1 expression in 5xFAD mouse is lower than WT mouse across age. Whole tissue lysates were obtained from WT (C57BL6) and 5xFAD male mouse hippocampi (**A-B**) and cortices (**C-D**) of different ages as indicated – 2 months (2M), 4M to 10M. **A,C**, Representative

immunoblots for TIMP-1 from hippocampal (**A**) and cortical (**C,** ladder was run in the middle for 2M-5M and 6M-8M blots and cut through the ladder for convenience during blot development) whole tissues where two consecutive lanes indicate protein levels in two separate animals of each age group. **B,D,** Densitometric analysis for TIMP-1 normalized with GAPDH or Actin as the loading control from hippocampal (**B**) and cortical (**D**) blots, showing relative TIMP-1 expression in 5xFAD mice w.r.t. WT mice. For N=6 mice/group for **B** and N= 4 mice/group for **D**; two-tailed unpaired t-test, mean±s.e.m.*P<0.05, **P<0.01, ***P<0.001 and ****P<0.0001.

Figure S2: TIMP-1 injection improves cognitive performance of 5xFAD mice in behavioral tests. A-B, In open-field test (OFT), the mean velocity of the mouse in cm/sec (**A**) and the time spent in the inner zone in sec (**B**) of the OFT arena during 10 min duration. One-way ANOVA, Tukey's post hoc, mean±s.e.m. **C-D**, In Elevated Plus-maze (EPM) test, latency (sec) to the closed arms on Day-1 (Initial transfer latency, ITL) and on Day-2 (Retention transfer latency, RTL), tracked for each mouse (**C**) and their difference ITL-RTL in sec for each group (**D**). Two-tailed unpaired t-test for **C** (@P<0.0001, $P<0.001) and One-way ANOVA, Tukey's post hoc for **D**; mean±s.e.m. **E**, Day-2 results of Novel Object Recognition (NOR) test showing Exploration time (sec) with Familiar (F) versus Novel (N) object within each group for the 5 min duration of the test where the each connecting line tracks the exploration time for each mouse between F and N. Two-tailed unpaired t-test, mean±s.e.m. *P<0.05, **P<0.01, ***P<0.001 and ****P<0.0001; ns, not significant. Number of animals in each test is given in Supplementary Table-1.

Figure S3. TIMP-1 injection in 5xFAD mice clears Aβ plaques. A, Representative immunofluorescence images for $A\beta_{1-42}$ deposits (red) in WT, 5xFAD and 5xFAD+TIMP-1 mouse brains in the hippocampal CA1 region, 14 days post TIMP-1 (5 ng) treatment. Nuclei stained by Hoechst (blue). Left panel shows 10x images (scale bar – 50 µm) where white box indicates region-of-interest in the CA1 region that were zoomed-in at 40x (scale bar – 50 µm). **B-C**, Plaque burden percentage (**B**, *P = 0.0054 versus WT, $^{\#}$P = 0.0051 versus 5xFAD) and plaque number (**C**, *P = 0.0004 versus WT, $^{\#}$P = 0.0004 versus 5xFAD) were calculated from area and number of Aβ puncta respectively. N = 3 mice/group, n=3 slices/mouse brain. One-way ANOVA, Tukey's post hoc, mean±s.e.m.

Figure S4. TIMP-1 restricts apoptosis in 5xFAD mouse. A, Representative immunofluorescence images following TUNEL assay in 5xFAD mice sections showing apoptotic cells (red puncta highlighted with white arrow) colocalized with the nuclei (blue) imaged at 40x (scale bar – 25 µm), alongside WT and 5xFAD+TIMP-1 images. In merged image panel, the red box demarcates the nuclei zoomed-in for better viewing of the colocalization in the inset. **B,** Percentage of TUNEL positive cells for N = 3 mice/group, n=3-4 slices/mouse brain, 250 cells/slice at 20x. One-way ANOVA, Tukey's post hoc, mean±s.e.m.; *p<0.0231, #p<0.0162. **C**, Representative western blots for pH2Ax(S139) from hippocampal tissue along with respective actin. **D,** Densitometric analyses for pH2Ax showing fold change w.r.t. WT. N=3 mice/group; One-way ANOVA, Tukey's post hoc, mean±s.e.m.; *P<0.05, #P<0.05. **E,G**, Representative immunofluorescence images for pH2ax (red) and nuclei (blue) in the

hippocampus (**E**) and in cortex (**G**); scale bar- 10 µm. White box shown in the merged panel demarcates a single nucleus zoomed for higher magnification viewing (inset). **F,H,** Percentage of pH2Ax positive nuclei in hippocampus (**F**, *p=0.0367, #p=0.0246) and cortex (**H**, *p<0.0001, #p < 0.0001), N=3 mice/group. One-way ANOVA, Tukey's post hoc, mean±s.e.m.

Figure S5: TIMP-1 injection in 5xFAD mice protects against impaired autophagy. A-B, E-F, I-J, M-N, Representative immunofluorescence images for pULK1(S757) (**A**, Hpc; **B**, Ctx), p62 (**E**, Hpc; **F**, Ctx), LC3B (**I**, Hpc; **J**, Ctx) and LAMP1 (**M**, Hpc; **N**, Ctx), 14 days post TIMP-1 injection in 5xFAD mice. White boxes in MERGED panel demarcates the region-of-interest for higher magnification images shown in the right panel. **C-D, G-H, K-L, O-P**, CTCF for pULK1(S757) (**C**, Hpc; **D,** Ctx), p62 (**G**, Hpc; **H,** Ctx), LC3B (**K,** Hpc**; L,** Ctx) and LAMP1 (**O,** Hpc**; P,** Ctx**)**. N=3 mice/group, n=50 cells/mouse from hippocampus (Hpc) and 100 cells/mouse from cortex (Ctx) quantified from 40x images, One-way ANOVA, Tukey's post hoc, mean±s.e.m.*P<0.0001, #P<0.0001; Scale bar=25 µm.

Figure S6: TIMP-1 corrects SNAP25 and PSD95 levels in 5xFAD mouse but not that of Homer1 and Synaptophysin. A,C, Representative immunofluorescence images for SNAP25 (green, **A**) and PSD95 (red, **C**) in coronal sections of WT, 5xFAD and 5xFAD+TIMP-1 cortex; scale bar, 30 µm at 40x magnification (white box indicates the region selected for further zoom-in). Zoom-in merged images are shown with nuclei stained with Hoechst (blue); scale bar, 15µm. **B,D**, CTCF calculated forfor SNAP25 (**B**) and PSD95 (**D**), N = 3 animals/group, n = 150 cells/animal from Cortex (Ctx) quantified from 40x images; One-way ANOVA, Tukey's post hoc, mean±s.e.m. *P<0.0001, #P<0.0001 for **B** and **D**. **E-F,** Representative immunoblots for Homer1 **(E**) and Synaptophysin1 (SYNAP**, F**) from whole hippocampal (Hpc) tissue of mice 14 days post TIMP-1 injection. N = animal number.

Figure S7: TIMP-1 improves CREB activity in the hippocampus of 5xFAD mice. A, Representative immunoblots for pCREB(Ser133) and CREB from hippocampal whole tissue isolated 14 days post TIMP-1 treatment. **B**, Densitometric analyses for pCREB/CREB showing fold change w.r.t. WT group. N=4 mice/group; One-way ANOVA, Tukey's post hoc, mean±s.e.m.;*P<0.0015, #P<0.0024.

Figure S8: TIMP-1 improves BDNF and related signaling at cortical synapses of 5xFAD mice. WB data from cortical synaptosomes 14 days post TIMP-1 treatment. Representative blots for Pro-BDNF (**A**), TrkB (**C**), pAkt(S473) (**F**), pAkt(T308) (**H**) and pERK1/2 (**J**) with corresponding loading controls. Densitometric analyses and normalized fold change w.r.t. WT for Pro-BDNF (**B**), fl-TrkB (**D**), t-TrkB (**E**), pAkt(S473)/Akt (**G**), pAkt(t308)/Akt (**I**), pERK1/ERK2 (**K**) and pERK2/ERK2 (**L**). N=6 independent synaptosome isolations/group, One-way ANOVA, Tukey's post hoc for **B**; N=4 independent synaptosome isolations/group, One-way ANOVA, Tukey's post hoc for **D,E,G,I,K,L**. Each synaptosome batch (N) isolated from 6-7 animals for each group. All data expressed as mean±s.e.m. Fl-TrkB, Full-length TrkB; t-TrkB,

truncated TrkB. Also see *P<0.05 versus WT, #P<0.05 versus 5xFAD, ns=not significant. Exact P values for this figure are given in Supplementary Table 1.

Supplementary Table 1: Overview statistics

REFERENCES

1 Verkhratsky, A., Zorec, R. & Parpura, V. Stratification of astrocytes in healthy and diseased brain. *Brain Pathol***27**, 629-644, doi:10.1111/bpa.12537 (2017).

2 Arranz, A. M. & De Strooper, B. The role of astroglia in Alzheimer's disease: pathophysiology and clinical implications. *Lancet Neurol***18**, 406-414, doi:S1474-4422(18)30490-3 (2019).

3 Escartin, C. *et al.* Reactive astrocyte nomenclature, definitions, and future directions. *Nat Neurosci***24**, 312-325, doi:10.1038/s41593-020-00783-4(2021).

4 Liddelow, S. A. & Barres, B. A. Reactive Astrocytes: Production, Function, and Therapeutic Potential. *Immunity***46**, 957-967, doi:S1074-7613(17)30234-0 (2017).

5 Habib, N. *et al.* Disease-associated astrocytes in Alzheimer's disease and aging. *Nat Neurosci***23**, 701-706, doi:10.1038/s41593-020-0624-8 (2020).

6 Hasel, P., Rose, I. V. L., Sadick, J. S., Kim, R. D. & Liddelow, S. A. Neuroinflammatory astrocyte subtypes in the mouse brain. *Nat Neurosci***24**, 1475-1487, doi:10.1038/s41593-021-00905-6 (2021).

7 Saha, P., Sarkar, S., Paidi, R. K. & Biswas, S. C. TIMP-1: A key cytokine released from activated astrocytes protects neurons and ameliorates cognitive behaviours in a rodent model of Alzheimer's disease. *Brain Behav Immun***87**, 804-819, doi:S0889-1591(19)31210-3 (2020).

8 Ashutosh, Chao, C., Borgmann, K., Brew, K. & Ghorpade, A. Tissue inhibitor of metalloproteinases-1 protects human neurons from staurosporine and HIV-1-induced apoptosis: mechanisms and relevance to HIV-1-associated dementia. *Cell Death Dis***3**, e332, doi:10.1038/cddis.2012.54 (2012).

9 Gardner, J. & Ghorpade, A. Tissue inhibitor of metalloproteinase (TIMP)-1: the TIMPed balance of matrix metalloproteinases in the central nervous system. *J Neurosci Res***74**, 801-806, doi:10.1002/jnr.10835 (2003).

10 Suryadevara, R. *et al.* Regulation of tissue inhibitor of metalloproteinase-1 by astrocytes: links to HIV-1 dementia. *Glia***44**, 47-56, doi:10.1002/glia.10266 (2003).

11 Althoff, G. E. *et al.* Long-term expression of tissue-inhibitor of matrix metalloproteinase-1 in the murine central nervous system does not alter the morphological and behavioral phenotype but alleviates the course of experimental allergic encephalomyelitis. *Am J Pathol***177**, 840-853, doi:10.2353/ajpath.2010.090918(2010).

12 Tuna, G., Yener, G. G., Oktay, G., Islekel, G. H. & FG, K. I. Evaluation of Matrix Metalloproteinase-2 (MMP-2) and -9 (MMP-9) and Their Tissue Inhibitors (TIMP-1 and TIMP-2) in Plasma from Patients with Neurodegenerative Dementia. *J Alzheimers Dis***66**, 1265-1273, doi:10.3233/JAD-180752(2018).

13 Stetler-Stevenson, W. G. Tissue inhibitors of metalloproteinases in cell signaling: metalloproteinase-independent biological activities. *Sci Signal***1**, re6, doi:10.1126/scisignal.127re6 (2008).

14 Jung, K. K., Liu, X. W., Chirco, R., Fridman, R. & Kim, H. R. Identification of CD63 as a tissue inhibitor of metalloproteinase-1 interacting cell surface protein. *EMBO J***25**, 3934-3942, doi:7601281 (2006).

15 Zhang, J. *et al.* TIMP-1 and CD82, a promising combined evaluation marker for PDAC. *Oncotarget***8**, 6496-6512, doi:10.18632/oncotarget.14133 (2017).

16 Thevenard, J. *et al.* Low-density lipoprotein receptor-related protein-1 mediates endocytic clearance of tissue inhibitor of metalloproteinases-1 and promotes its cytokine-like activities. *PloS one***9**, e103839, doi:10.1371/journal.pone.0103839 (2014).

17 Grunwald, B., Schoeps, B. & Kruger, A. Recognizing the Molecular Multifunctionality and Interactome of TIMP-1. *Trends Cell Biol***29**, 6-19, doi:S0962-8924(18)30144-2 (2019).

18 Park, S. A. *et al.* TIMP-1 mediates TGF-beta-dependent crosstalk between hepatic stellate and cancer cells via FAK signaling. *Sci Rep***5**, 16492, doi:10.1038/srep16492 (2015).

19 Lee, S. Y. *et al.* TIMP-1 modulates chemotaxis of human neural stem cells through CD63 and integrin signalling. *Biochem J***459**, 565-576, doi:10.1042/BJ20131119 (2014).

20 Nicaise, A. M., Johnson, K. M., Willis, C. M., Guzzo, R. M. & Crocker, S. J. TIMP-1 Promotes Oligodendrocyte Differentiation Through Receptor-Mediated Signaling. *Mol Neurobiol***56**, 3380-3392, doi:10.1007/s12035-018-1310-7 (2019).

21 Forner, S. *et al.* Systematic phenotyping and characterization of the 5xFAD mouse model of Alzheimer's disease. *Sci Data***8**, 270, doi:10.1038/s41597-021-01054-y (2021).

22 Forte, D. *et al.* The tissue inhibitor of metalloproteinases-1 (TIMP-1) promotes survival and migration of acute myeloid leukemia cells through CD63/PI3K/Akt/p21 signaling. *Oncotarget***8**, 2261-2274, doi:10.18632/oncotarget.13664 (2017).

23 Sanphui, P. & Biswas, S. C. FoxO3a is activated and executes neuron death via Bim in response to beta-amyloid. *Cell Death Dis***4**, e625, doi:10.1038/cddis.2013.148 (2013).

24 Akhter, R., Sanphui, P. & Biswas, S. C. The essential role of p53-up-regulated modulator of apoptosis (Puma) and its regulation by FoxO3a transcription factor in beta-amyloid-induced neuron death. *J Biol Chem***289**, 10812-10822, doi:S0021-9258(20)40343-6 (2014).

25 Lambert, E. *et al.* Tissue inhibitor of metalloproteinases-1 signalling pathway leading to erythroid cell survival. *Biochem J***372**, 767-774, doi:10.1042/BJ20030187 (2003).

26 Nalluri, S. *et al.* TIMP-1 Inhibits Apoptosis in Lung Adenocarcinoma Cells via Interaction with Bcl-2. *PLoS One***10**, e0137673, doi:10.1371/journal.pone.0137673 (2015).

27 Saleem, S. & Biswas, S. C. Tribbles Pseudokinase 3 Induces Both Apoptosis and Autophagy in Amyloid-beta-induced Neuronal Death. *J Biol Chem***292**, 2571-2585, doi:10.1074/jbc.M116.744730 (2017).

28 Saha, A., Saleem, S., Paidi, R. K. & Biswas, S. C. BH3-only proteins Puma and Beclin1 regulate autophagic death in neurons in response to Amyloid-beta. *Cell Death Discov***7**, 356, doi:10.1038/s41420-021-00748-x (2021).

29 Gharami, K. & Biswas, S. C. Glutamate treatment mimics LTP- and LTD-like biochemical activity in viable synaptosome preparation. *Neurochem Int***134**, 104655, doi:S0197-0186(19)30532-7 (2020).

30 Subramanian, J., Savage, J. C. & Tremblay, M. E. Synaptic Loss in Alzheimer's Disease: Mechanistic Insights Provided by Two-Photon in vivo Imaging of Transgenic Mouse Models. *Front Cell Neurosci***14**, 592607, doi:10.3389/fncel.2020.592607 (2020).

31 Koffie, R. M., Hyman, B. T. & Spires-Jones, T. L. Alzheimer's disease: synapses gone cold. *Mol Neurodegener***6**, 63, doi:10.1186/1750-1326-6-63 (2011).

32 Pelucchi, S., Stringhi, R. & Marcello, E. Dendritic Spines in Alzheimer's Disease: How the Actin Cytoskeleton Contributes to Synaptic Failure. *Int J Mol Sci***21**, doi:10.3390/ijms21030908 (2020).

33 Mizuno, K. Signaling mechanisms and functional roles of cofilin phosphorylation and dephosphorylation. *Cell Signal***25**, 457-469, doi:S0898-6568(12)00304-X (2013).

34 Zagrebelsky, M., Tacke, C. & Korte, M. BDNF signaling during the lifetime of dendritic spines. *Cell Tissue Res***382**, 185-199, doi:10.1007/s00441-020-03226-5 (2020).

35 Edelmann, E., Lessmann, V. & Brigadski, T. Pre- and postsynaptic twists in BDNF secretion and action in synaptic plasticity. *Neuropharmacology***76 Pt C**, 610-627, doi:10.1016/j.neuropharm.2013.05.043 (2014).

36 Amidfar, M., de Oliveira, J., Kucharska, E., Budni, J. & Kim, Y. K. The role of CREB and BDNF in neurobiology and treatment of Alzheimer's disease. *Life Sci***257**, 118020, doi:S0024-3205(20)30770-0 (2020).

37 Minichiello, L. TrkB signalling pathways in LTP and learning. *Nat Rev Neurosci***10**, 850-860, doi:10.1038/nrn2738(2009).

38 Diogenes, M. J. *et al.* Enhancement of LTP in aged rats is dependent on endogenous BDNF. *Neuropsychopharmacology***36**, 1823-1836, doi:10.1038/npp.2011.64 (2011).

39 Whitlock, J. R., Heynen, A. J., Shuler, M. G. & Bear, M. F. Learning induces long-term potentiation in the hippocampus. *Science***313**, 1093-1097, doi:313/5790/1093 (2006).

40 Bradley, C. A. *et al.* A pivotal role of GSK-3 in synaptic plasticity. *Front Mol Neurosci***5**, 13, doi:10.3389/fnmol.2012.00013 (2012).

41 Jaworski, T., Banach-Kasper, E. & Gralec, K. GSK-3beta at the Intersection of Neuronal Plasticity and Neurodegeneration. *Neural Plast***2019**, 4209475, doi:10.1155/2019/4209475 (2019).

42 McAlpine, C. S. *et al.* Astrocytic interleukin-3 programs microglia and limits Alzheimer's disease. *Nature***595**, 701-706, doi:10.1038/s41586-021-03734-6 (2021).

43 Price, B. R., Johnson, L. A. & Norris, C. M. Reactive astrocytes: The nexus of pathological and clinical hallmarks of Alzheimer's disease. *Ageing Res Rev***68**, 101335, doi:S1568-1637(21)00082-9 (2021).

44 Py, N. A. *et al.* Differential spatio-temporal regulation of MMPs in the 5xFAD mouse model of Alzheimer's disease: evidence for a pro-amyloidogenic role of MT1-MMP. *Front Aging Neurosci***6**, 247, doi:10.3389/fnagi.2014.00247 (2014).

45 Corsi, G. I. *et al.* The transcriptomic landscape of neurons carrying PSEN1 mutations reveals changes in extracellular matrix components and non-coding gene expression. *Neurobiol Dis***178**, 105980, doi:S0969-9961(22)00372-2 (2022).

46 Zhao, G. X., Pan, H., Ouyang, D. Y. & He, X. H. The critical molecular interconnections in regulating apoptosis and autophagy. *Ann Med***47**, 305-315, doi:10.3109/07853890.2015.1040831 (2015).

47 Scheff, S. W., Price, D. A., Schmitt, F. A. & Mufson, E. J. Hippocampal synaptic loss in early Alzheimer's disease and mild cognitive impairment. *Neurobiol Aging***27**, 1372-1384, doi:S0197-4580(05)00283-6 (2006).

48 Reddy, P. H. *et al.* Abnormal mitochondrial dynamics and synaptic degeneration as early events in Alzheimer's disease: implications to mitochondria-targeted antioxidant therapeutics. *Biochim Biophys Acta***1822**, 639-649, doi:10.1016/j.bbadis.2011.10.011 (2012).

49 Kommaddi, R. P. *et al.* Abeta mediates F-actin disassembly in dendritic spines leading to cognitive deficits in Alzheimer's disease. *J Neurosci***38**, 1085-1099, doi:10.1523/JNEUROSCI.2127-17.2017 (2018).

50 Bamburg, J. R. *et al.* ADF/Cofilin-actin rods in neurodegenerative diseases. *Curr Alzheimer Res***7**, 241-250, doi:CAR -62 (2010).

51 Deng, Y. *et al.* Partial Amelioration of Synaptic and Cognitive Deficits by Inhibiting Cofilin Dephosphorylation in an Animal Model of Alzheimer's Disease. *J Alzheimers Dis***53**, 1419-1432, doi:10.3233/JAD-160167 (2016).

52 Liu, X. *et al.* Overexpression of REST Causes Neuronal Injury and Decreases Cofilin Phosphorylation in Mice. *J Alzheimers Dis***87**, 873-886, doi:10.3233/JAD-210285 (2022).

53 Woo, J. A. *et al.* Slingshot-Cofilin activation mediates mitochondrial and synaptic dysfunction via Abeta ligation to beta1-integrin conformers. *Cell Death Differ***22**, 921-934, doi:10.1038/cdd.2015.5 (2015).

54 Shimohama, S., Kamiya, S., Taniguchi, T., Akagawa, K. & Kimura, J. Differential involvement of synaptic vesicle and presynaptic plasma membrane proteins in Alzheimer's disease. *Biochem Biophys Res Commun***236**, 239-242, doi:S0006-291X(97)96940-0 (1997).

55 Clarke, M. T. M. *et al.* CSF synaptic protein concentrations are raised in those with atypical Alzheimer's disease but not frontotemporal dementia. *Alzheimers Res Ther***11**, 105, doi:10.1186/s13195-019-0564-2 (2019).

56 Brinkmalm, G. *et al.* A Parallel Reaction Monitoring Mass Spectrometric Method for Analysis of Potential CSF Biomarkers for Alzheimer's Disease. *Proteomics Clin Appl***12**, doi:10.1002/prca.201700131 (2018).

57 Borba, E. M. *et al.* Brain-Derived Neurotrophic Factor Serum Levels and Hippocampal Volume in Mild Cognitive Impairment and Dementia due to Alzheimer Disease. *Dement Geriatr Cogn Dis Extra***6**, 559-567, doi:10.1159/000450601 (2016).

58 Lima Giacobbo, B. *et al.* Brain-Derived Neurotrophic Factor in Brain Disorders: Focus on Neuroinflammation. *Mol Neurobiol***56**, 3295-3312, doi:10.1007/s12035-018-1283-6 (2019).

59 Maher, F. O., Clarke, R. M., Kelly, A., Nally, R. E. & Lynch, M. A. Interaction between interferon gamma and insulin-like growth factor-1 in hippocampus impacts on the ability of rats to sustain long-term potentiation. *J Neurochem***96**, 1560-1571, doi:JNC3664 (2006).

60 Singh, A., Jones, O. D., Mockett, B. G., Ohline, S. M. & Abraham, W. C. Tumor Necrosis Factor-alpha-Mediated Metaplastic Inhibition of LTP Is Constitutively Engaged in an Alzheimer's Disease Model. *J Neurosci***39**, 9083-9097, doi:10.1523/JNEUROSCI.1492-19.2019 (2019).

61 Magnowska, M. *et al.* Transient ECM protease activity promotes synaptic plasticity. *Sci Rep***6**, 27757, doi:10.1038/srep27757 (2016).

62 Okulski, P. *et al.* TIMP-1 abolishes MMP-9-dependent long-lasting long-term potentiation in the prefrontal cortex. *Biol Psychiatry***62**, 359-362, doi:S0006-3223(06)01142-5 (2007).

63 Citri, A. & Malenka, R. C. Synaptic plasticity: multiple forms, functions, and mechanisms. *Neuropsychopharmacology***33**, 18-41, doi:1301559 (2008).

64 Peineau, S. *et al.* A systematic investigation of the protein kinases involved in NMDA receptor-dependent LTD: evidence for a role of GSK-3 but not other serine/threonine kinases. *Mol Brain***2**, 22, doi:10.1186/1756-6606-2-22 (2009).

65 Zhang, L. *et al.* Hydrogen-rich saline controls remifentanil-induced hypernociception and NMDA receptor NR1 subunit membrane trafficking through GSK-3beta in the DRG in rats. *Brain Res Bull***106**, 47-55, doi:10.1016/j.brainresbull.2014.05.005 (2014).

66 Chen, P., Gu, Z., Liu, W. & Yan, Z. Glycogen synthase kinase 3 regulates N-methyl-D-aspartate receptor channel trafficking and function in cortical neurons. *Mol Pharmacol***72**, 40-51, doi:mol.107.034942 (2007).

67 Pei, J. J. *et al.* Distribution, levels, and activity of glycogen synthase kinase-3 in the Alzheimer disease brain. *J Neuropathol Exp Neurol***56**, 70-78, doi:10.1097/00005072-199701000-00007 (1997).

68 Hooper, C. *et al.* Glycogen synthase kinase-3 inhibition is integral to long-term potentiation. *Eur J Neurosci***25**, 81-86, doi:EJN5245 (2007).

69 Perez-Costas, E., Gandy, J. C., Melendez-Ferro, M., Roberts, R. C. & Bijur, G. N. Light and electron microscopy study of glycogen synthase kinase-3beta in the mouse brain. *PLoS One***5**, e8911, doi:10.1371/journal.pone.0008911 (2010).

70 Atkins, W. M. Biological messiness vs. biological genius: Mechanistic aspects and roles of protein promiscuity. *J Steroid Biochem Mol Biol***151**, 3-11, doi:S0960-0760(14)00209-X (2015).

71 Zhong, F., Liu, L., Wei, J. L. & Dai, R. P. Step by Step Golgi-Cox Staining for Cryosection. *Front Neuroanat***13**, 62, doi:10.3389/fnana.2019.00062 (2019).

FIGURE 1

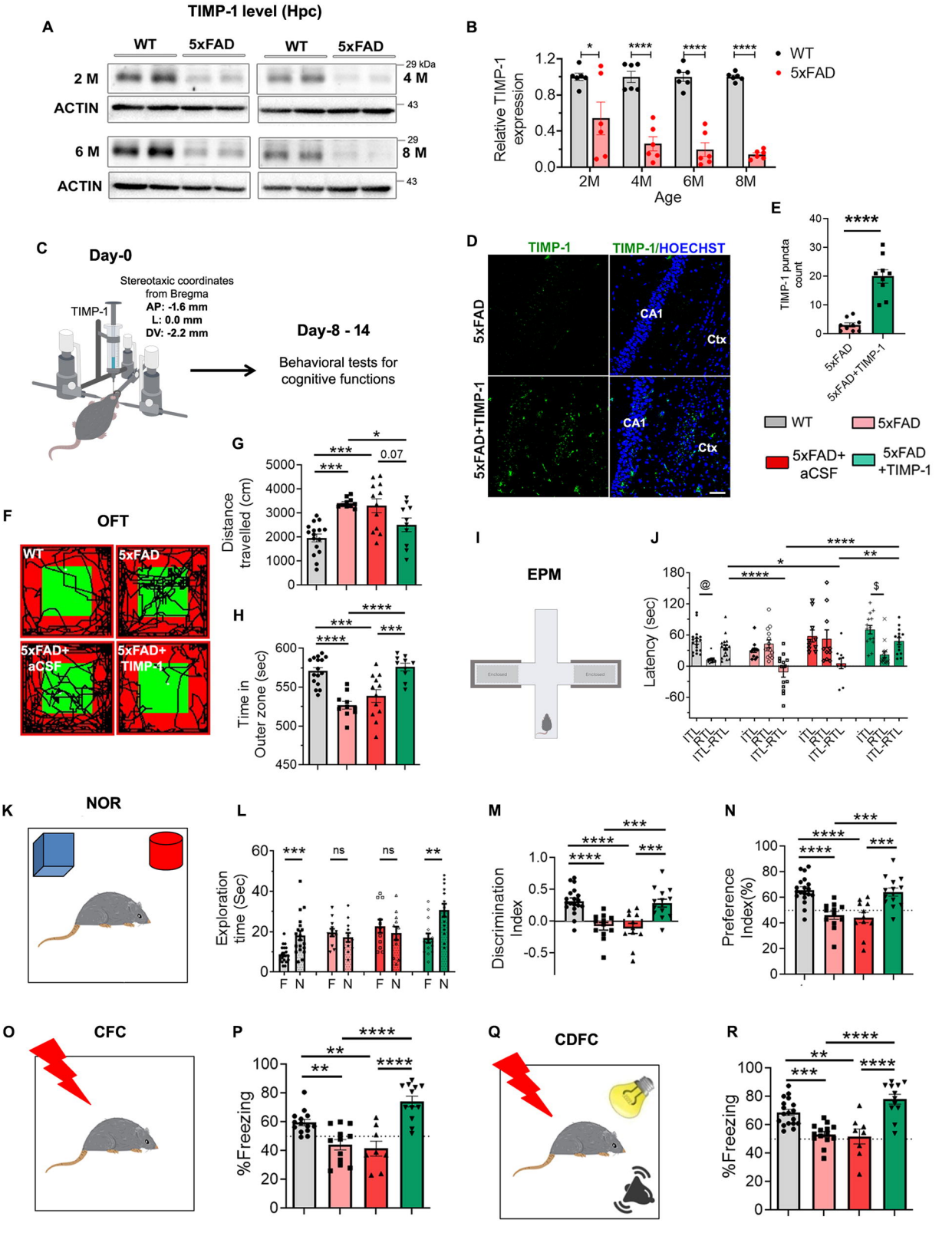
A
TIMP-1 level (Hpc)
WT
5xFAD
WT
5xFAD
2 M
4 M
ACTIN
6 M
8 M
ACTIN
29 kDa
43
29
43
B
Relative TIMP-1 expression
Age
2M
4M
6M
8M
WT
5xFAD
C
Day-0
Stereotaxic coordinates from Bregma
AP: -1.6 mm
L: 0.0 mm
DV: -2.2 mm
TIMP-1
Day-8 - 14
Behavioral tests for cognitive functions
D
TIMP-1
TIMP-1/HOECHST
5xFAD
5xFAD+TIMP-1
CA1
Ctx
E
TIMP-1 puncta count
5xFAD
5xFAD+TIMP-1
WT
5xFAD
5xFAD+ aCSF
5xFAD +TIMP-1
F
OFT
WT
5xFAD
5xFAD+ aCSF
5xFAD+ TIMP-1
G
Distance travelled (cm)
H
Time in Outer zone (sec)
I
EPM
Enclosed
J
Latency (sec)
iTL
RTL
iTL-RTL
K
NOR
L
Exploration time (Sec)
F
N
M
Discrimination Index
N
Preference Index(%)
O
CFC
P
%Freezing
Q
CDFC
R
%Freezing

FIGURE 2

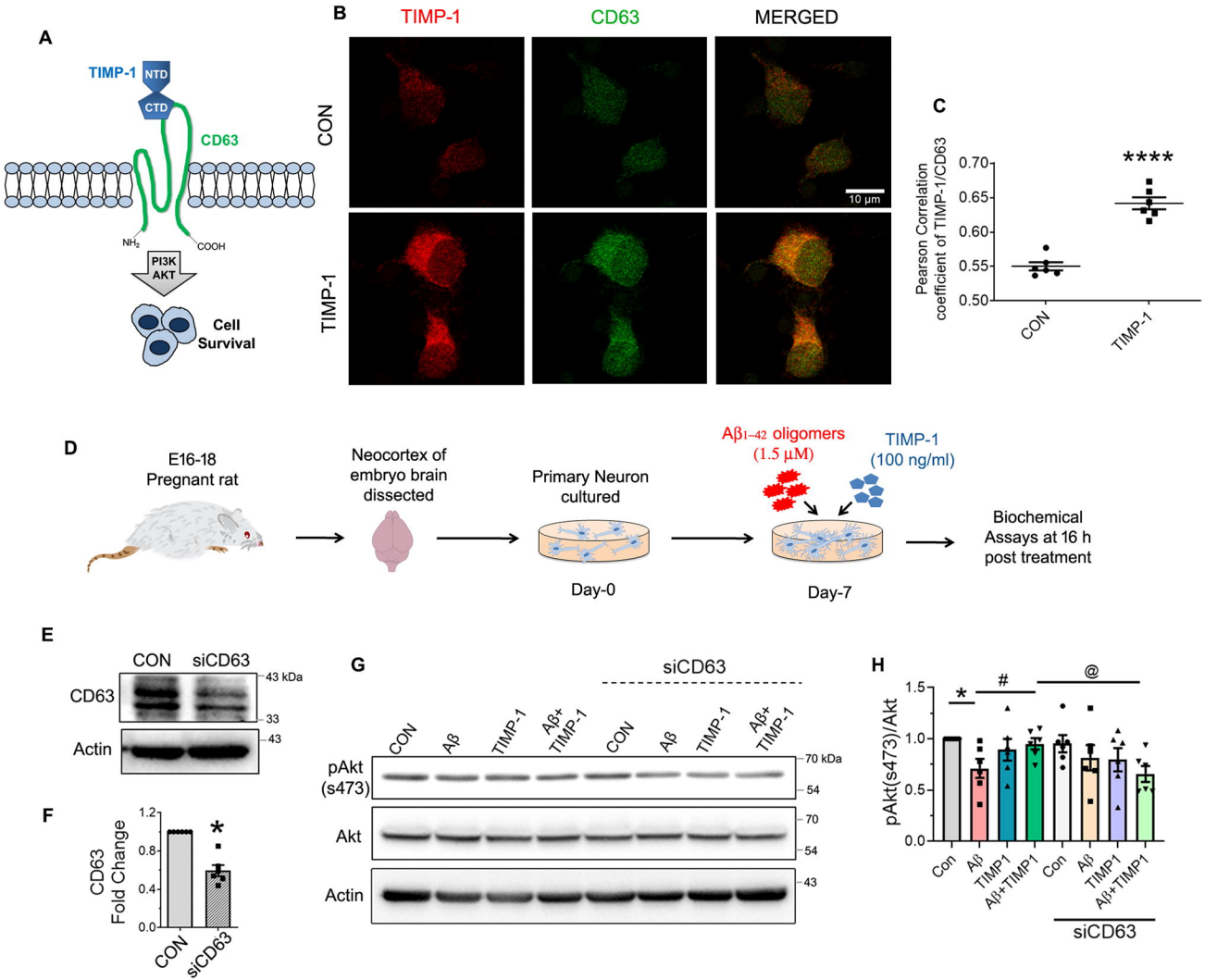
A
TIMP-1
NTD
CTD
CD63
NH2
COOH
PI3K
AKT
Cell Survival
B
TIMP-1
CD63
MERGED
CON
TIMP-1
10 µm
C
Pearson Correlation coefficient of TIMP-1/CD63
0.70
0.65
0.60
0.55
0.50
****
CON
TIMP-1
D
E16-18 Pregnant rat
Neocortex of embryo brain dissected
Primary Neuron cultured
Day-0
Aβ1–42 oligomers (1.5 µM)
TIMP-1 (100 ng/ml)
Day-7
Biochemical Assays at 16 h post treatment
E
CON
siCD63
CD63
43 kDa
33
Actin
43
F
CD63 Fold Change
1.2
0.8
0.4
0.0
*
CON
siCD63
G
siCD63
CON
Aβ
TIMP-1
Aβ+ TIMP-1
CON
Aβ
TIMP-1
Aβ+ TIMP-1
pAkt (s473)
70 kDa
54
Akt
70
54
Actin
43
H
pAkt(s473)/Akt
1.5
1.0
0.5
0.0
*
#
@
Con
Aβ
TIMP1
Aβ+TIMP1
Con
Aβ
TIMP1
Aβ+TIMP1
siCD63

FIGURE 3

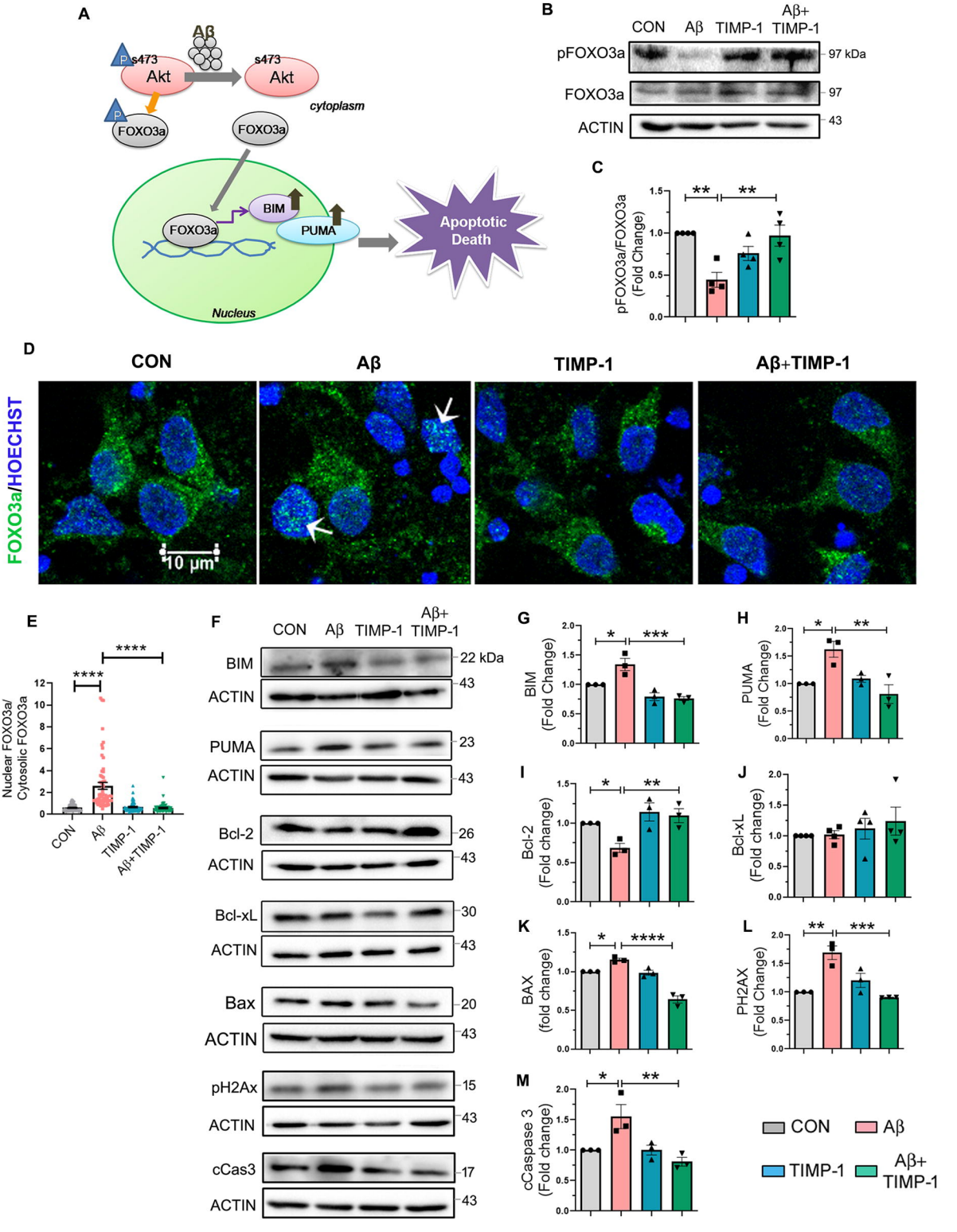
A
Aβ
s473
Akt
s473
Akt
cytoplasm
FOXO3a
FOXO3a
FOXO3a
BIM
PUMA
Apoptotic Death
Nucleus
B
CON
Aβ
TIMP-1
Aβ+ TIMP-1
pFOXO3a
FOXO3a
ACTIN
97 kDa
97
43
C
pFOXO3a/FOXO3a (Fold Change)
D
CON
Aβ
TIMP-1
Aβ+TIMP-1
FOXO3a/HOECHST
10 μm
E
Nuclear FOXO3a/ Cytosolic FOXO3a
CON
Aβ
TIMP-1
Aβ+TIMP-1
F
CON
Aβ
TIMP-1
Aβ+ TIMP-1
BIM
ACTIN
22 kDa
PUMA
Bcl-2
Bcl-xL
Bax
pH2Ax
cCas3
G
BIM (Fold Change)
H
PUMA (Fold Change)
I
Bcl-2 (Fold change)
J
Bcl-xL (Fold change)
K
BAX (fold change)
L
PH2AX (Fold Change)
M
cCaspase 3 (Fold change)
CON
Aβ
TIMP-1
Aβ+ TIMP-1

FIGURE 4

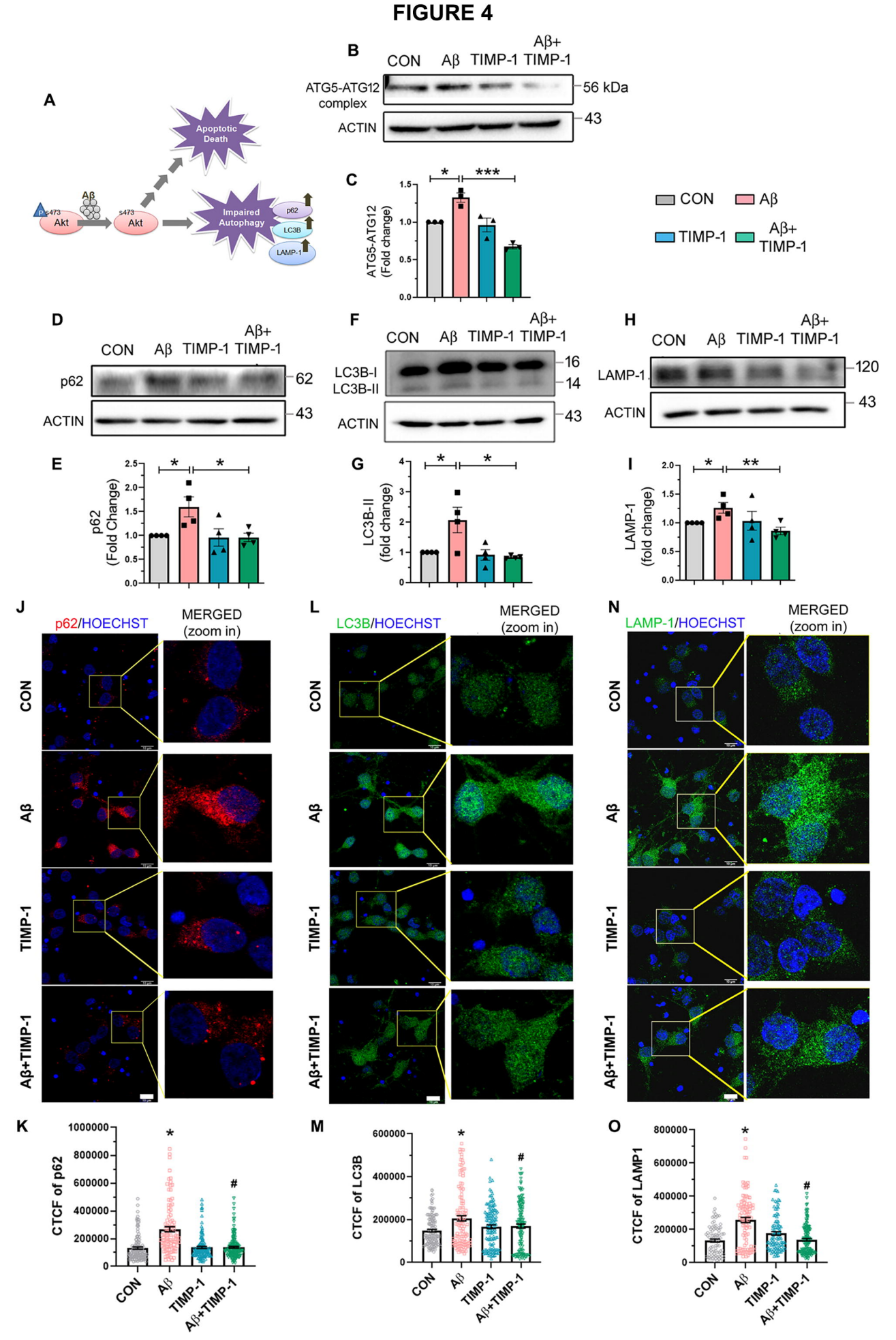
A
Apoptotic Death
Aβ
P-s473 Akt
s473 Akt
Impaired Autophagy
p62
LC3B
LAMP-1
B
CON
Aβ
TIMP-1
Aβ+ TIMP-1
ATG5-ATG12 complex
56 kDa
ACTIN
43
C
ATG5-ATG12 (Fold change)
CON
Aβ
TIMP-1
Aβ+ TIMP-1
D
p62
62
ACTIN
43
E
p62 (Fold Change)
F
LC3B-I
LC3B-II
16
14
G
LC3B-II (fold change)
H
LAMP-1
120
I
LAMP-1 (fold change)
J
p62/HOECHST
MERGED (zoom in)
L
LC3B/HOECHST
N
LAMP-1/HOECHST
K
CTCF of p62
M
CTCF of LC3B
O
CTCF of LAMP1

FIGURE 5

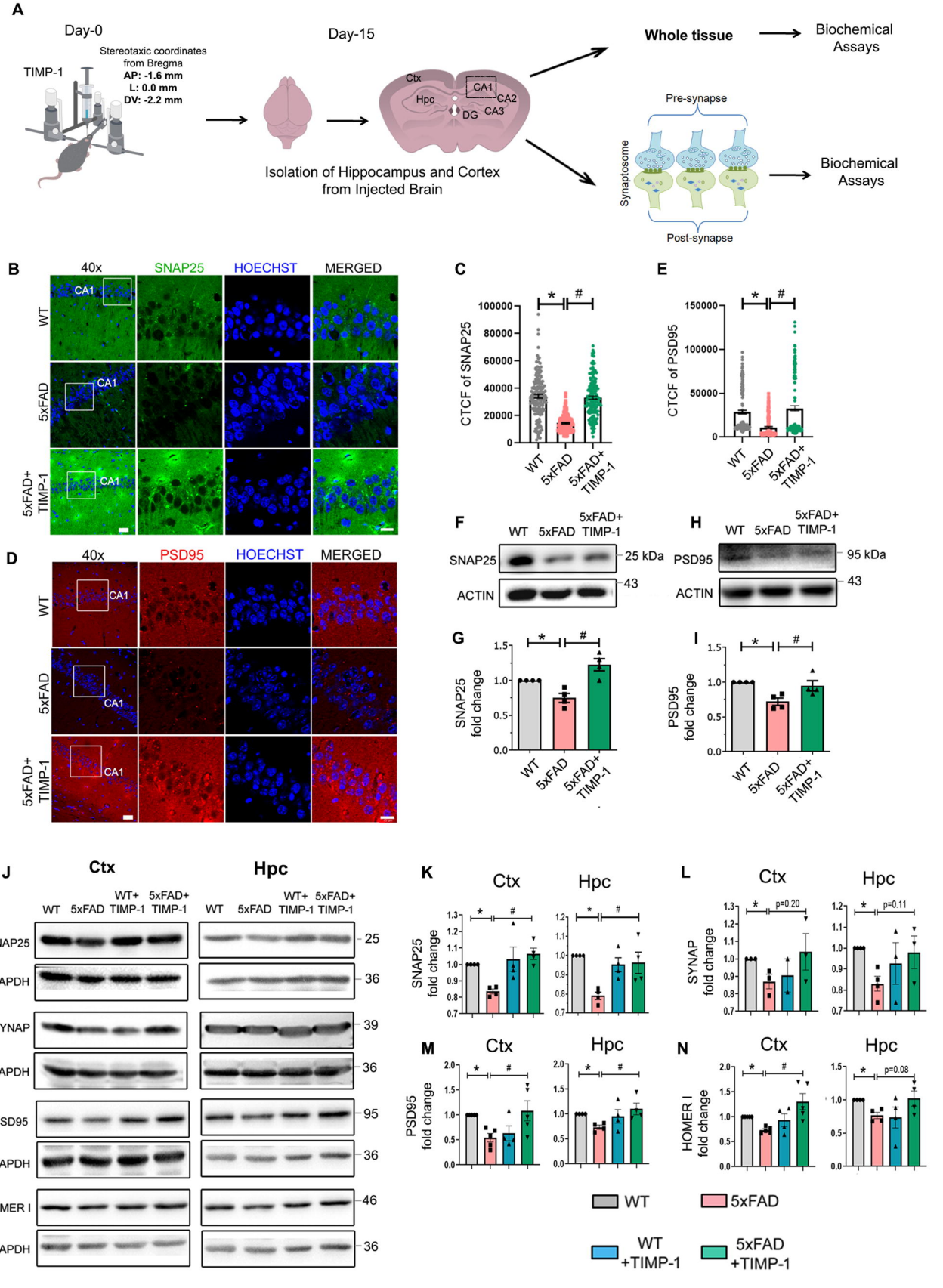
A
Day-0
Day-15
TIMP-1
Stereotaxic coordinates from Bregma
AP: -1.6 mm
L: 0.0 mm
DV: -2.2 mm
Ctx
Hpc
CA1
CA2
CA3
DG
Isolation of Hippocampus and Cortex from Injected Brain
Whole tissue
Biochemical Assays
Pre-synapse
Synaptosome
Post-synapse
Biochemical Assays
B
40x
SNAP25
HOECHST
MERGED
WT
5xFAD
5xFAD+ TIMP-1
CA1
C
CTCF of SNAP25
WT
5xFAD
5xFAD+ TIMP-1
E
CTCF of PSD95
D
PSD95
F
SNAP25
ACTIN
25 kDa
43
H
PSD95
95 kDa
G
SNAP25 fold change
I
PSD95 fold change
J
Ctx
Hpc
WT+ TIMP-1
5xFAD+ TIMP-1
SYNAP
HOMER I
K
L
SYNAP fold change
p=0.20
p=0.11
M
N
HOMER I fold change
p=0.08
WT
5xFAD
WT +TIMP-1
5xFAD +TIMP-1

FIGURE 6

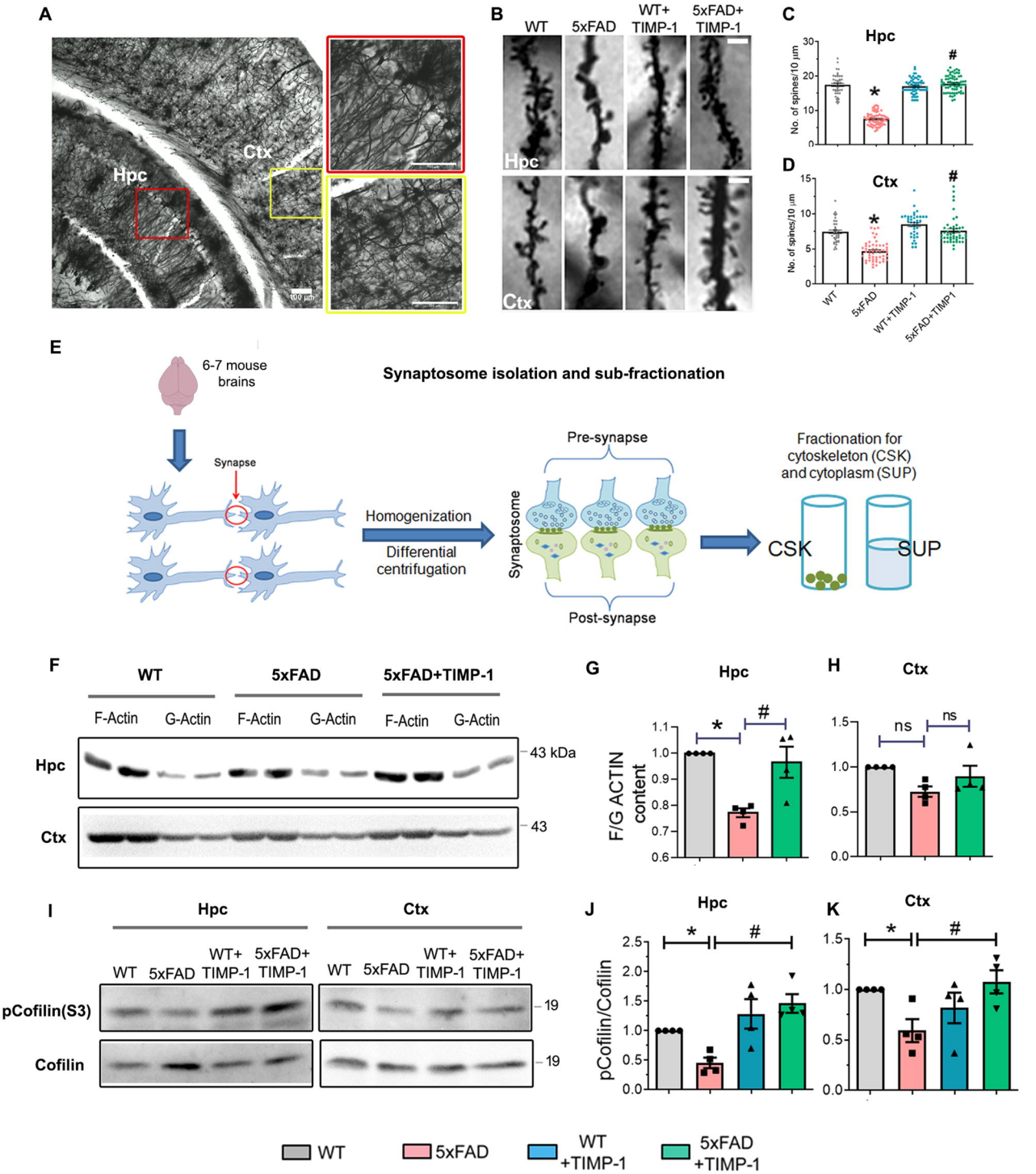
A
Hpc
Ctx
100 µm
B
WT
5xFAD
WT+ TIMP-1
5xFAD+ TIMP-1
Hpc
Ctx
C
Hpc
No. of spines/10 µm
D
Ctx
WT
5xFAD
WT+TIMP-1
5xFAD+TIMP1
E
6-7 mouse brains
Synaptosome isolation and sub-fractionation
Synapse
Homogenization
Differential centrifugation
Pre-synapse
Synaptosome
Post-synapse
Fractionation for cytoskeleton (CSK) and cytoplasm (SUP)
CSK
SUP
F
WT
5xFAD
5xFAD+TIMP-1
F-Actin
G-Actin
Hpc
Ctx
43 kDa
43
G
Hpc
F/G ACTIN content
H
Ctx
ns
I
Hpc
Ctx
WT
5xFAD
WT+ TIMP-1
5xFAD+ TIMP-1
pCofilin(S3)
Cofilin
19
J
Hpc
pCofilin/Cofilin
K
Ctx
WT
5xFAD
WT +TIMP-1
5xFAD +TIMP-1

FIGURE 7

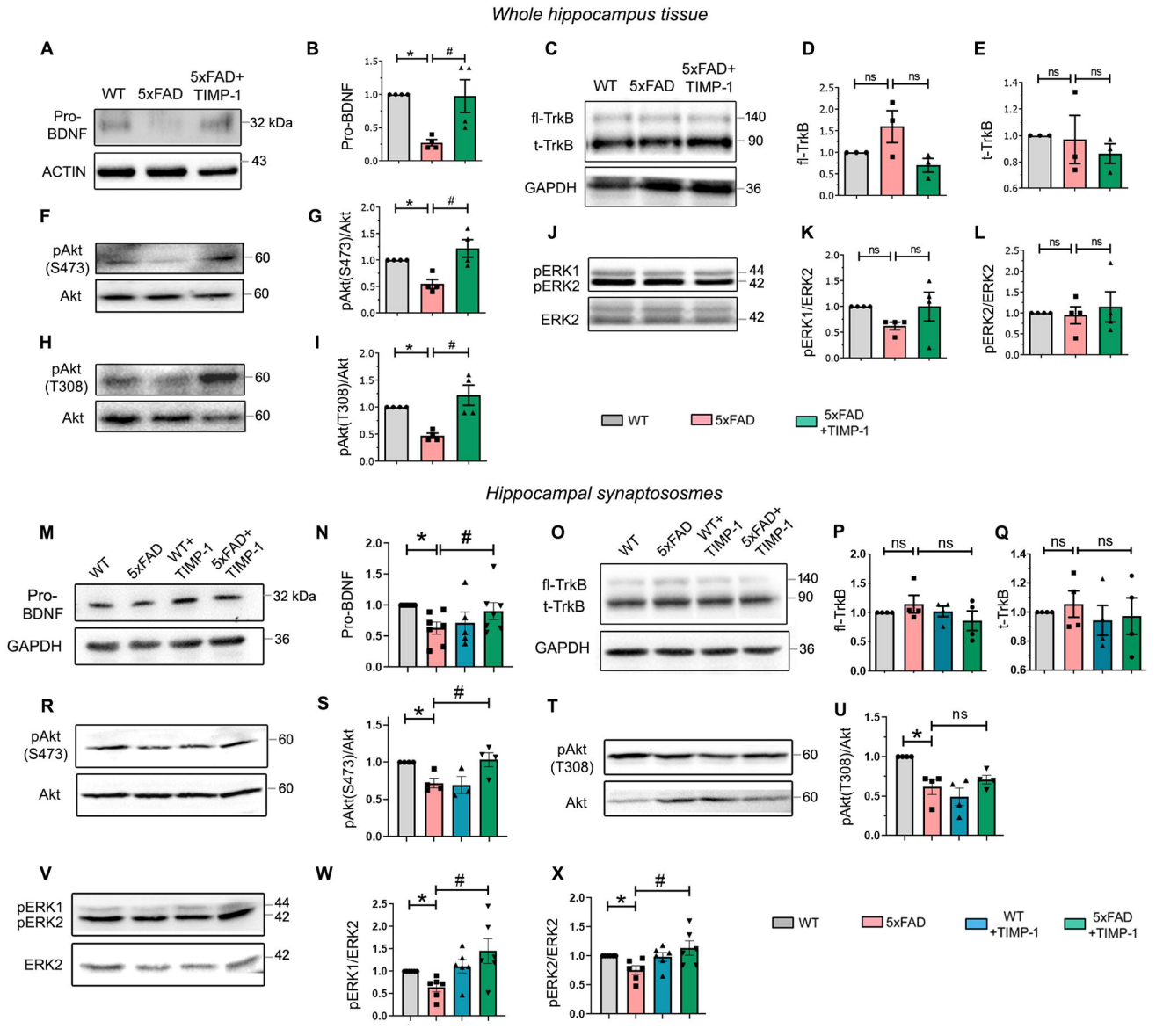
Whole hippocampus tissue
A
WT
5xFAD
5xFAD+ TIMP-1
Pro-BDNF
32 kDa
ACTIN
43
B
Pro-BDNF
C
fl-TrkB
t-TrkB
GAPDH
140
90
36
D
fl-TrkB
E
t-TrkB
F
pAkt (S473)
Akt
60
G
pAkt(S473)/Akt
H
pAkt (T308)
I
pAkt(T308)/Akt
J
pERK1
pERK2
ERK2
44
42
K
pERK1/ERK2
L
pERK2/ERK2
ns
*
#
WT
5xFAD
5xFAD +TIMP-1
Hippocampal synaptosomes
M
WT+ TIMP-1
N
O
P
Q
R
S
T
U
V
W
X

FIGURE 8

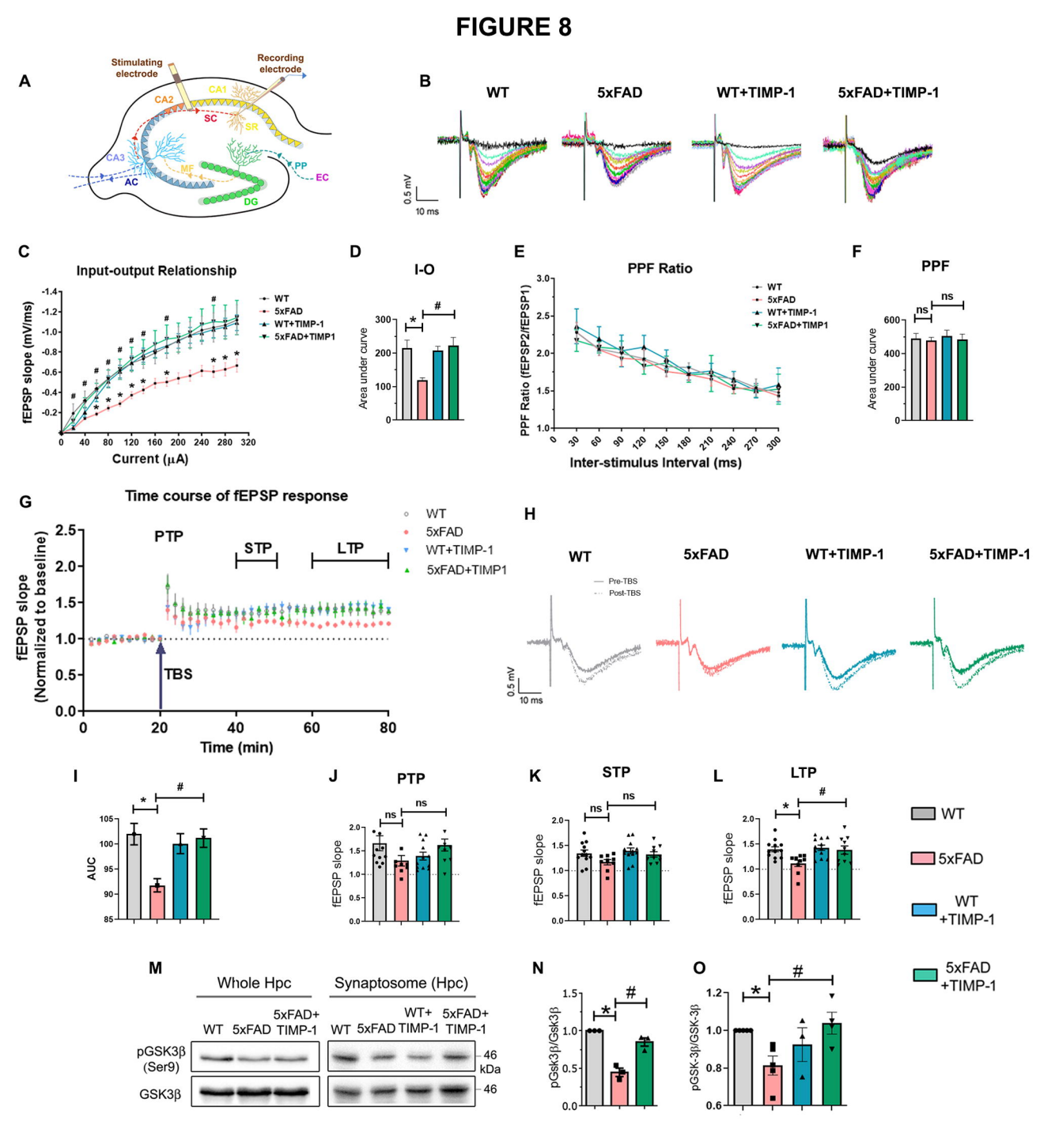
A
Stimulating electrode
Recording electrode
CA1
CA2
SC
SR
CA3
MF
PP
EC
AC
DG
B
WT
5xFAD
WT+TIMP-1
5xFAD+TIMP-1
0.5 mV
10 ms
C
Input-output Relationship
fEPSP slope (mV/ms)
Current (μA)
WT
5xFAD
WT+TIMP-1
5xFAD+TIMP1
D
I-O
Area under curve
E
PPF Ratio
PPF Ratio (fEPSP2/fEPSP1)
Inter-stimulus Interval (ms)
F
PPF
Area under curve
ns
G
Time course of fEPSP response
fEPSP slope (Normalized to baseline)
PTP
STP
LTP
TBS
Time (min)
H
WT
5xFAD
WT+TIMP-1
5xFAD+TIMP-1
Pre-TBS
Post-TBS
I
AUC
J
PTP
fEPSP slope
K
STP
L
LTP
M
Whole Hpc
Synaptosome (Hpc)
pGSK3β (Ser9)
GSK3β
46 kDa
N
pGsk3β/Gsk3β
O
pGSK-3β/GSK-3β